Bachelorarbeit

Zur Erlangung des akademischen Grades Bachelor of Science (B.Sc.)

Investigation of the lattice dynamics of Ge and LiF using the linear-response approach implemented in the `exciting` code

eingereicht von: Tim Heinl

Gutachter/innen: PD Pasquale Pavone

Prof. Claudia Draxl

Eingereicht am Institut für Physik der Humboldt-Universität zu Berlin am:
03. September 2024

Abstract

This work presents *ab-initio* calculations for the phonon-dispersion relations for the semiconductor germanium and the insulator lithium fluoride. The ground-state calculations were performed using density-functional theory implemented in the **exciting** code. The density-functional perturbation theory, a linear-response technique, was used as the method for the calculation of the phonon properties. Results of the influence of the exchange-correlation functionals **LDA**, **PBE**, and **PBEsol** on the calculations of phonon-dispersion relations are presented as well as test results, occured problems, and problem solving approaches for the **exciting** code.

Contents

1 Introduction **1**

2 Theoretical background **3**

2.1 Dynamics of a crystal lattice 3

2.1.1 Crystal structure and reciprocal space 3

2.1.2 Adiabatic and harmonic approximation 4

2.1.3 Equations of motion 6

2.1.4 First Brillouin zone 7

2.1.5 Classification of the dispersion branches 7

2.1.6 Quantum-mechanical phonons 8

2.2 Total energy 9

2.2.1 Density-functional theory 10

2.2.2 Kohn-Sham equations 11

2.2.3 Exchange-correlation functionals 12

2.2.4 Self-consistent calculations 12

2.3 Density-functional perturbation theory 13

2.3.1 Dynamical matrix of polar materials 14

2.4 Numerical solution 15

2.4.1 Expansion into basis functions 15

2.4.2 The software package **`exciting`** 16

3 Results **19**

3.1 Computational details 19

3.2 Structure optimization 21

3.3 Phonon properties 22

3.3.1 Germanium 25

3.3.2 Lithium fluoride 32

4 Conclusions and Outlook **40**

Bibliography **42**

A `species` files **46**

B Phonon properties of Ge **49**

B.1 `LDA` 50

B.2 `PBEsol` 51

B.3 `PBE` 52

C Phonon properties of LiF **53**

C.1 `LDA` 54

C.2 `PBEsol` 55

C.3 `PBE` 56

Chapter 1

Introduction

In this thesis, the lattice dynamics of germanium and lithium fluoride was investigated. For this purpose, the phonon-dispersion relations, the phonon density of states, and specific values of the phonon frequencies at highly-symmetrical points of the first Brillouin zone were calculated and analyzed for the two materials.

Germanium is one of the semimetals in the periodic table and is classified as a semiconductor. It was once the leading material in electrical technology before it was replaced by silicon [1]. Nevertheless, it is still used, *e.g.*, in high-frequency technology, detector technology, and infrared optics. Elementary Ge crystallizes in the diamond structure and is a non-polar material with covalent atomic bonding [2]. Lithium fluoride, the lithium salt of hydrofluoric acid, crystallizes in the rock-salt structure and is a polar material with ionic bonding [3]. LiF is used as a flux in the manufacture of glass and ceramics or in radiation detectors for ionizing radiation in thermoluminescence dosimeters [4].

The ground-state calculations which were performed in this work are based on density-functional theory [5, 6] as implemented in the full-potential all-electron computer package **`exciting`** [7]. Furthermore, the density-functional perturbation theory [8], a linear-response technique, was used to calculate the phonon properties. In calculations based on density-functional theory, so-called exchange-correlation functionals [5] are required. Two classes of these were used for our calculations, the local-density approximation (**`LDA`**) [6] and the generalized gradient approximation (**`GGA`**) [6], represented by **`PBE`** [6] and **`PBEsol`** [9].

Two main objectives were pursued in this work. The first objective was to calculate the phonon-dispersion relations, phonon density of states, and phonon frequencies of Ge and LiF. These significantly determine a variety of solid-state properties, such as the specific heat, the thermal expansion, the dielectric properties of ionic crystals, the superconductivity of metals and many more [10]. Within this context, the purpose was to obtain well converged data for the basic lattice-dynamical prop-

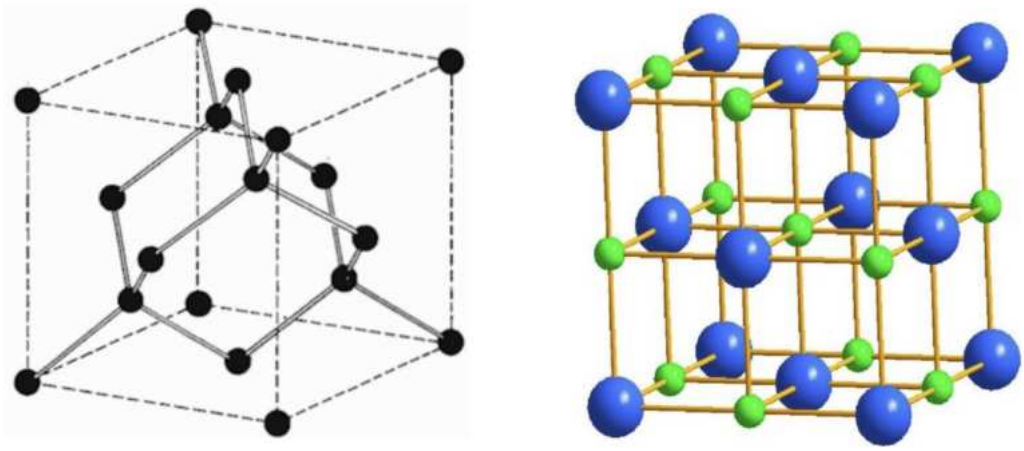

Figure 1.1: Schematic representation of the diamond structure (left) for germanium from Ref. [11] and the rock-salt structure (right) for lithium fluoride from Ref. [12]. The lithium cations are shown in blue and the fluorine anions in green.

erties, in particular, to investigate the effect of using various exchange-correlation functionals.

The second objective was to test and verify the implementation of the linear-response approach within density-functional perturbation theory in the **exciting** code. Ge was chosen as a non-polar material with covalent bonding and semiconductor properties. LiF was chosen as a polar insulator with ionic bonding. The schematic representation of the crystal structures of Ge and LiF can be seen in Fig. 1.1. These fundamentally different materials were used to test the capabilities of the **exciting** code and identify potential problems.

This thesis is organized as follows. In Chapter 2, the theoretical foundations are explained and the software package **exciting** is described. In Chapter 3, the phonon-dispersion relations, the phonon density of states, and the phonon frequencies calculated in this work are presented and discussed. Finally, in Chapter 4, the results are evaluated and conclusions are drawn.

Chapter 2

Theoretical background

In this chapter, the physical concepts, properties, and theories fundamental to this work are briefly introduced and the used software package is conceptually described. At the beginning, the core ideas of the physical description of the dynamics of a crystal lattice are presented and the concept of the phonons is constructed on this foundation. This is followed by a description of the density-functional theory (**DFT**) and density-functional perturbation theory (**DFPT**). Finally, the software package **exciting** is examined in more detail.

2.1 Dynamics of a crystal lattice

The content of this section is based on Refs. [10, 13].

2.1.1 Crystal structure and reciprocal space

Crystal structure

An ideal crystal is understood as a strictly periodic repetition of identical structural elements extending over the entire three-dimensional space and it is described by specifying the structural unit, which is referred to as the basis, and the instruction of the sequence of structural units, which leads to a spatial lattice. So-called Bravais lattices are often used for the specification of the spatial lattice, on which the structural units of the crystal are arranged. A Bravais lattice in three-dimensional space consists of all points:

$$\mathbf{R}_n \equiv \mathbf{R}_{n_1,n_2,n_3} = n_1\,\mathbf{a}_1 + n_2\,\mathbf{a}_2 + n_3\,\mathbf{a}_3\,, \qquad \text{with} \qquad n \equiv (n_1, n_2, n_3)\,, \tag{2.1}$$

where n_1, n_2, and n_3 are integers and the vectors $\mathbf{a}_1$, $\mathbf{a}_2$, and $\mathbf{a}_3$ are not coplanar. They are referred to as primitive lattice vectors. The spatial lattice is spanned by

them. Their lengths a_1, a_2, and a_3 are referred to as lattice constants. A parallelepiped, the so-called primitive cell, is spanned by the primitive lattice vectors $\mathbf{a}_1$, $\mathbf{a}_2$, and $\mathbf{a}_3$. The primitive cell is the smallest unit cell that fills the entire space through periodic repetition. Its volume is given by:

$$\Omega = |\mathbf{a}_1 \cdot (\mathbf{a}_2 \times \mathbf{a}_3)| \,. \tag{2.2}$$

Reciprocal space

A reciprocal lattice can be assigned to each Bravais lattice, in which its primitive lattice vectors, $\{\mathbf{b}_j\}$, are perpendicular to the primitive vectors, $\{\mathbf{a}_i\}$, of the real lattice. The primitive lattice vectors, $\{\mathbf{b}_j\}$, are formed by the following rule:

$$\mathbf{b}_1 = \frac{2\pi}{\Omega}(\mathbf{a}_2 \times \mathbf{a}_3) \,, \quad \mathbf{b}_2 = \frac{2\pi}{\Omega}(\mathbf{a}_3 \times \mathbf{a}_1) \,, \quad \mathbf{b}_3 = \frac{2\pi}{\Omega}(\mathbf{a}_1 \times \mathbf{a}_2) \,. \tag{2.3}$$

This means that each lattice vector of the reciprocal space can be written as:

$$\mathbf{G} = k_1 \, \mathbf{b}_1 + k_2 \, \mathbf{b}_2 + k_3 \, \mathbf{b}_3 \,, \tag{2.4}$$

with integer triple k_1, k_2, and k_3. With the help of reciprocal lattice vectors, families of parallel lattice planes can be described uniquely, because each reciprocal lattice vector is perpendicular to a family of parallel lattice planes of the Bravais lattice. The identification of families of parallel lattice planes in the Bravais lattice with lattice vectors of reciprocal space is crucial for the determination of the dispersion relation of phonons.

2.1.2 Adiabatic and harmonic approximation

The description of the vibrations of the atoms of a solid is very complex. To simplify this, the adiabatic and harmonic approximations are usually employed.

Adiabatic approximation

Because of the reaction principle, the forces that electrons and nuclei exert on each other are equal and opposite. The quantitative relationship $M_{\text{nuc}}\ddot{R}_{\text{nuc}} \cong m_{\text{e}}\ddot{r}_{\text{e}}$ can be established, with M_{nuc} for the mass of a nucleus, $\ddot{R}_{\text{nuc}}$ for the acceleration of this nucleus, m_{e} for the mass of an electron, and $\ddot{r}_{\text{e}}$ for the acceleration of this electron. From this it is easy to see that the heavy nuclei move significantly slower than the light electrons. The idea of the adiabatic approximation is based on this: The electrons can adapt adiabatically to the slow motion of the heavy nuclei at any point in time or, to put it another way, the motion of the electrons can be considered

to be decoupled from the motion of the nuclei. Thus, the total energy of a system of many nuclei and electrons results from the sum of the electronic ("potential") contribution, U_{el}, the total electrostatic energy due to the nuclei only, U_{nuc}, and the kinetic energy of the nuclei T_{nuc} in:

$$E_{\mathrm{tot}} = U_{\mathrm{el}} + U_{\mathrm{nuc}} + T_{\mathrm{nuc}} \equiv U + \sum_{\mathrm{nuc}} \frac{\mathbf{P}_{\mathrm{nuc}}^2}{2M_{\mathrm{nuc}}} \ . \tag{2.5}$$

Here, $U = U_{\mathrm{el}} + U_{\mathrm{nuc}}$ is the total potential energy which is acting on the nuclei.

Harmonic approximation

The exact expression of the potential energy $U = U_{\mathrm{el}} + U_{\mathrm{nuc}}$ can be very complicated. To simplify the description, in many cases it is useful to approximate the potential around the equilibrium positions of the atomic nuclei by a harmonic potential. Therefore, consider the position of an atom within the n-th lattice cell described by

$$\mathbf{X}_{n\alpha} = \mathbf{R}_n + \boldsymbol{\tau}_\alpha + \mathbf{u}_{n\alpha} \ , \tag{2.6}$$

where $\mathbf{R}_n$ indicates the n-th point of the Bravais lattice, $\boldsymbol{\tau}_\alpha$ the equilibrium position of the α-th atom in the n-th lattice cell and $\mathbf{u}_{n\alpha}$ the displacement of the α-th atom in the n-th lattice cell from its equilibrium position.

The potential energy U depends on the full nuclear configuration $\{\mathbf{X}_{n\alpha}\}$. To approximate this harmonically around equilibrium, U is first Taylor-expanded around the equilibrium position $\{\mathbf{X}^0_{n\alpha} = \mathbf{R}_n + \boldsymbol{\tau}_\alpha\}$:

$$U \equiv U(\{\mathbf{X}_{n\alpha}\}) = U(\{\mathbf{X}^0_{n\alpha}\}) + \sum_{n,\alpha} \mathbf{u}_{n\alpha} \cdot \left.\frac{\partial U}{\partial \mathbf{u}_{n\alpha}}\right|_{\mathrm{eq}} + \frac{1}{2} \sum_{n,m,\alpha,\beta} \mathbf{u}_{n\alpha} \cdot \left.\frac{\partial^2 U}{\partial \mathbf{u}_{n\alpha}\, \partial \mathbf{u}_{m\beta}}\right|_{\mathrm{eq}} \cdot \mathbf{u}_{m\beta} + \cdots \tag{2.7}$$

Here, all derivatives are calculated at the equilibrium configuration. The first term corresponds to the equilibrium energy and can be set to zero or to a reference constant. The linear term disappears, as this term sums up all the forces that all atoms exert on an atom, and these just disappear for the equilibrium state. If the Taylor expansion is terminated after the quadratic term, the harmonic potential is obtained:

$$U_{\mathrm{harm}} = U_0 + \frac{1}{2} \sum_{n,m,\alpha,\beta} \mathbf{u}_{n\alpha} \cdot \left.\frac{\partial^2 U}{\partial \mathbf{u}_{n\alpha}\, \partial \mathbf{u}_{m\beta}}\right|_{\mathrm{eq}} \cdot \mathbf{u}_{m\beta} \ . \tag{2.8}$$

Here, U_0 denotes the equilibrium energy. The second derivatives of the potential calculated at equilibrium are referred to as *coupling* or *inter-atomic force constants*:

$$C^{m\beta j}_{n\alpha i} = \left.\frac{\partial^2 U}{\partial u_{n\alpha i}\, \partial u_{m\beta j}}\right|_{\mathrm{eq}} \ . \tag{2.9}$$

2.1.3 Equations of motion

With the help of the harmonic potential in Eq. (2.8) and the laws of classical mechanics, the relationship between the oscillation frequencies and the wave vectors of the lattice oscillations can be established. According to Newton's laws, the sum of the inertial forces and coupling forces must be zero for the displacement of an atom α in the lattice cell n in direction i:

$$M_\alpha \frac{\partial^2 u_{n\alpha i}}{\partial t^2} + \sum_{m,\beta,j} C_{n\alpha i}^{m\beta j}\, u_{m\beta j} = 0\,. \tag{2.10}$$

For a solid with N_{cell} lattice cells and N_{at} atoms per unit cell, $\widetilde{d} = 3\,N_{\mathrm{cell}}\,N_{\mathrm{at}}$ differential equations result. Considering the immense size N_{cell} for a solid, the solution seems impossible. For periodic structures, however, an approach can be chosen in which the displacements $u_{n\alpha i}$ are interpreted as plane waves with respect to the cell coordinates:

$$u_{n\alpha i} = \frac{1}{\sqrt{M_\alpha}}\, A_{\alpha i}(\mathbf{q})\, \mathrm{e}^{\iota(\mathbf{q}\cdot\mathbf{R}_{\mathrm{n}} - \omega \mathrm{t})}\,. \tag{2.11}$$

Notice, that these plane waves are only defined at the lattice points $\mathbf{R}_n$. Using this approach in Eq. (2.10) leads to:

$$-\omega^2 A_{\alpha i}(\mathbf{q}) + \sum_{\beta,j}\sum_{m} \frac{1}{\sqrt{M_\alpha M_\beta}}\, C_{n\alpha i}^{m\beta j}\, e^{\iota\mathbf{q}\cdot(\mathbf{R}_m - \mathbf{R}_n)}\, A_{\beta j}(\mathbf{q}) = 0\,. \tag{2.12}$$

Due to the translation invariance, the terms in the sum are only dependent on $\mathbf{R}_m - \mathbf{R}_n$. Eq. (2.12) can be expressed in terms of the so-called dynamical matrix, defined as:

$$D_{\alpha i}^{\beta j}(\mathbf{q}) = \sum_{m} \frac{1}{\sqrt{M_\alpha M_\beta}}\, C_{n\alpha i}^{m\beta j}\, e^{\iota\mathbf{q}\cdot(\mathbf{R}_m - \mathbf{R}_n)}\,. \tag{2.13}$$

This definition can be used to set up a linear homogeneous system of equations of the order $d = 3\,N_{\mathrm{at}}$:

$$-\omega^2 A_{\alpha i}(\mathbf{q}) + \sum_{\beta,j} D_{\alpha i}^{\beta j}(\mathbf{q})\, A_{\beta j}(\mathbf{q}) = 0\,. \tag{2.14}$$

A linear homogeneous system of equations only has non-trivial solutions if the determinant of the coefficient matrix is zero:

$$\det\left\{\underline{\underline{\mathbf{D}}}(\mathbf{q}) - \omega^2\, \underline{\underline{\mathbf{1}}}\right\} = 0\,. \tag{2.15}$$

For each wave vector $\mathbf{q}$, this equation has exactly $d = 3\,N_{\mathrm{at}}$ solutions $\omega(\mathbf{q})$ for the oscillation frequencies. The dependence of the oscillation frequency on the wave vector is called the dispersion relation. The d different solutions are called branches of the dispersion relation.

2.1.4 First Brillouin zone

Looking at the derivation of the dispersion relation in the previous section, the question quickly arises, which wave vectors $\mathbf{q}$ should be considered in a reasonable way. Therefore, consider Eq. (2.13) and note that the coefficients $D_{\alpha i}^{\beta j}(\mathbf{q})$ of the dynamical matrix include sums over the phase factors $e^{\imath \mathbf{q}\cdot(\mathbf{R}_m - \mathbf{R}_n)}$. $\mathbf{R}_m$ and $\mathbf{R}_n$ are vectors of the Bravais lattice and since the relationship $\mathbf{G} \cdot \mathbf{R}_m = 2\pi \cdot (\text{integer})$ applies for each reciprocal lattice vector $\mathbf{G}$, it follows that

$$D_{\alpha i}^{\beta j}(\mathbf{q}) = D_{\alpha i}^{\beta j}(\mathbf{q} + \mathbf{G}) \,. \tag{2.16}$$

Thus, the solutions of Eq. (2.15) fulfill the condition:

$$\omega(\mathbf{q}) = \omega(\mathbf{q} + \mathbf{G}) \,. \tag{2.17}$$

Furthermore, two structurally similar waves with the only difference that they propagate in opposite directions can be converted into each other by time reversal, so the oscillation frequencies for $\mathbf{q}$ and $-\mathbf{q}$ must be the same:

$$\omega(\mathbf{q}) = \omega(-\mathbf{q}) \,. \tag{2.18}$$

Combining the findings in Eqs. (2.17) and (2.18), it can be seen that it is sufficient to consider the dispersion relation in the region of one reciprocal lattice vector. The first Brillouin zone can be used for this.

The calculations of many properties of solids, such as the total energy, require integrations over all possible $\mathbf{k}$-vectors of the first Brillouin zone. In order to keep the calculation time finite, the integrals are approximated by sums performed on a grid of $\mathbf{k}$-points.

2.1.5 Classification of the dispersion branches

In Section 2.1.3 it was worked out that for each wave vector $\mathbf{q}$ there are $d = 3\,N_{\text{at}}$ solutions $\omega(\mathbf{q})$ of the system of equations (see Eqs. (2.14) and (2.15)) and that these are referred to as branches of the dispersion relation. These branches can be classified. If a branch belongs to an oscillation in which neighboring oscillators oscillate in phase, it is referred to as an acoustic branch. If neighboring oscillators oscillate in anti-phase, this is called an optical branch. In a three-dimensional system with N_{at} atoms in the basis, there are 3 acoustic and $3\,N_{\text{at}} - 3$ optical branches. In addition to the classification according to acoustic and optical branches, a classification according to longitudinal and transverse branches is also common. At least for certain symmetry directions of the crystal system, deflections of the oscillations can

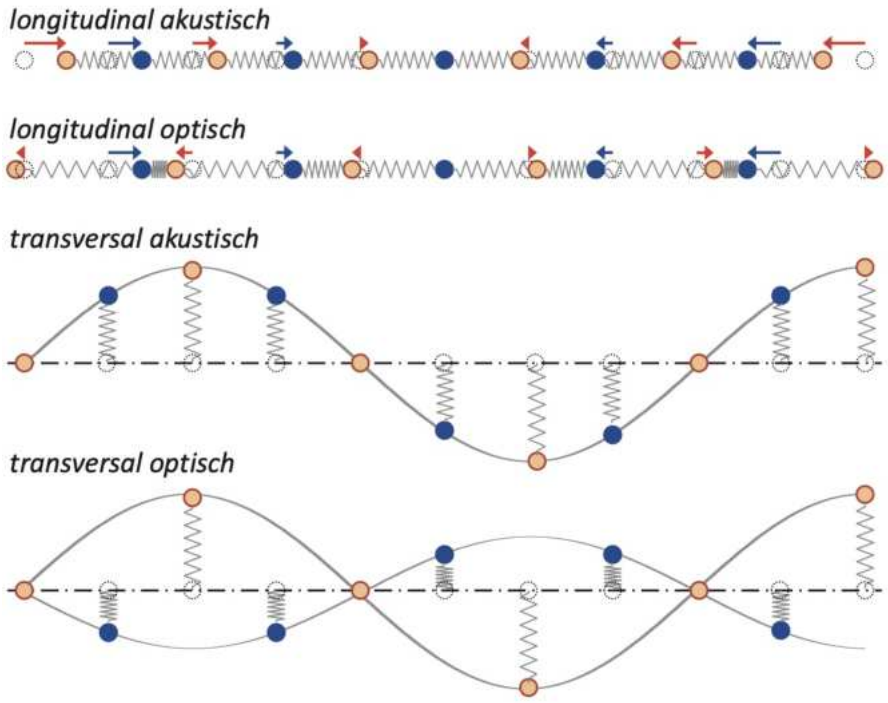

Figure 2.1: Longitudinal-acoustic (longitudinal *akustisch*), longitudinal-optical (longitudinal *optisch*), transverse-acoustic (transversal *akustisch*), and transverse-optical (transversal *optisch*) lattice vibrations in two dimensions (from Ref. [10]).

be either parallel or perpendicular to the wave vector $\mathbf{q}$. A distinction is therefore made between transverse-optical (`TO`), longitudinal-optical (`LO`), transverse-acoustic (`TA`), and longitudinal-acoustic (`LA`) branches. These are shown in Fig. 2.1.

2.1.6 Quantum-mechanical phonons

In the previous sections, the dynamics of the crystal lattice were treated classically. As a result of this consideration, a crystal can be understood as a sum of oscillators with natural frequencies $\omega_\nu(\mathbf{q})$, with $\nu = 1, ..., d$. However, there is also a quantum mechanical perspective on the dynamics of the crystal lattice, which will be explained below. For the mathematical consideration of the oscillations of a system of coupled oscillators, normal coordinates are usually introduced by a linear transformation. Within the harmonic approximation, these allow the equations of motion of uncoupled oscillators to be established. The frequency spectrum of the natural oscillations of the system of coupled oscillators corresponds to that of the normal oscillations of the uncoupled harmonic oscillators. The natural energies or natural

frequencies of the normal oscillations are given by the eigenvalues of the harmonic Hamilton operator:

$$\hat{H}_{\text{harm}} = \hat{T}_{\text{nuc}} + U_{\text{harm}} = \sum_{n,\alpha} \frac{1}{2M_\alpha} \hat{\mathbf{P}}_{n\alpha}^2 + U_{\text{harm}} \,, \tag{2.19}$$

with $\hat{T}_{\text{nuc}}$ for the kinetic energy of the lattice atoms and $U_{\text{el}}^{\text{harm}}$ for the harmonic approximation of the potential energy obtained in the adiabatic approximation. Now, the energy levels of a crystal consisting of $\tilde{N} \equiv N_{\text{cell}}\, N_{\text{at}}$ atoms can be specified by considering it as a system of $3\tilde{N}$ independent oscillators whose frequencies correspond to those of the $3\tilde{N}$ classical oscillation modes. A concrete oscillation state with the frequency $\omega_\nu(\mathbf{q})$ can only assume the following discrete energy values:

$$\left(n_{\mathbf{q}\nu} + \frac{1}{2}\right) \hbar\, \omega_\nu(\mathbf{q}) \,, \qquad n_{\mathbf{q}\nu} = 0, 1, 2, ... \,; \tag{2.20}$$

with $n_{\mathbf{q}\nu}$ for the occupation number of the normal oscillation with wave vector $\mathbf{q}$ in the dispersion branch ν. The total energy is then given by the sum of the energies of the individual modes as:

$$E_{\text{tot}} = \sum_{\mathbf{q}\nu} \left(n_{\mathbf{q}r} + \frac{1}{2}\right) \hbar\, \omega_\nu(\mathbf{q}) \,. \tag{2.21}$$

This result can be interpreted again as a normal oscillation with an occupation number $n_{\mathbf{q}\nu}$ and with a wave vector $\mathbf{q}$ in the dispersion branch ν. Each normal oscillation is called a phonon. Therefore, phonons are the quanta of the vibrational field of a crystal.

2.2 Total energy

In order to calculate the total energy defined in Eq. (2.5), one has to get the total electronic energy U_{el}. According to quantum mechanics, U_{el} is the energy of the many-electron system and can be obtained as:

$$U_{\text{el}} = \langle \Psi | \hat{H}_{\text{el}} | \Psi \rangle = \int d\mathbf{r}_1 ... d\mathbf{r}_N \, \Psi^*(\mathbf{r}_1, ..., \mathbf{r}_N)\, \hat{H}_{\text{el}}\, \Psi(\mathbf{r}_1, ..., \mathbf{r}_N) \,, \tag{2.22}$$

with Ψ for the total electronic wave function. $\hat{H}_{\text{el}}$ is the many-electron Hamiltonian defined as:

$$\hat{H}(\mathbf{r}_1, \mathbf{r}_2, ..., \mathbf{r}_N) = \hat{T} + \hat{V} + \hat{W} \equiv -\sum_i^N \frac{\nabla_i^2}{2} + \sum_i^N v(\mathbf{r}_i) + \frac{1}{2} \sum_{i \neq j}^N \frac{1}{|\mathbf{r}_i - \mathbf{r}_j|} \,, \tag{2.23}$$

where $\mathbf{r}_i$ describes the position of the i-th electron. The first term in Eq. (2.23), $\hat{T}$, is associated with the kinetic energy of the electrons. The second term, $\hat{V}$, describes the external Coloumb potential of the nuclei, where $v(\mathbf{r})$ is the contribution experienced by a specific electron, and the third term, $\hat{W}$, is associated with the Coloumb interaction of the electrons with each other.

The direct calculation of $U_{\rm el}$ in Eq. (2.22), however, is for a periodic system almost impossible, due to the huge number of electrons in the system. Therefore, alternative solutions have to be found. The most used alternative approach is the density-functional theory introduced in the next section. The information presented in this section relates to Refs. [5, 6].

2.2.1 Density-functional theory

The energy of any quantum system consisting of N electrons is obviously a functional of the corresponding wave function $\Psi(\mathbf{r}_1, ..., \mathbf{r}_N)$ (see, *e.g.*, Eq. (2.22)) and, therefore, depends on $3N$ variables. This makes the direct treatment of extended systems very difficult, if not impossible.

The idea of reducing the relevant degrees of freedom of an electron systems is the basic idea of the density-functional theory (`DFT`). Instead of using the wave function for the description of the system, one can use the ground-state (`GS`) electron density, $n_{\rm GS}(\mathbf{r})$, which depends only on 3 coordinates. The proof of this statement is given by the Hohenberg-Kohn (`HK`) theorem [14] which has a huge impact on numerical calculations in solid-state physics. As a consequence of the `HK` theorem, every physical property of an electron system can be considered a functional of $n_{\rm GS}(\mathbf{r})$. In particular this holds for the ground-state electron energy, which we called $U_{\rm el}$. In the following, for being closer to the specific literature on `DFT`, we set $U_{\rm el} \equiv E$. A very important corollary of the `HK` theorem, states that the functional $E[n]$ is minimized by $n_{\rm GS}(\mathbf{r})$. Then, if the functional $E[n]$ would be known, this corollary gives the way of calculating directly $n_{\rm GS}(\mathbf{r})$ *without* solving the many-electron problem with the standard quantum-mechanical approach.

The functional $E[n]$ can be written as

$$E[n] = \int d\mathbf{r}\, n(\mathbf{r})\, v(\mathbf{r}) + \langle \Psi[n] | \hat{T} + \hat{W} | \Psi[n] \rangle \equiv E_{\rm ext}[n] + F[n]\,. \tag{2.24}$$

The first term in the r.h.s. of Eq. (2.24), $E_{\rm ext}[n]$, depends directly on the electron density, but the other term only implicitly, which makes the functional $F[n]$ to be unknown. Formally, the minimization of $E[n]$ with respect to the density can be

obtained by solving the equation

$$\left.\frac{\delta E[n]}{\delta n(\mathbf{r})}\right|_{n_{\rm GS}} = v(\mathbf{r}) + \left.\frac{\delta F[n]}{\delta n(\mathbf{r})}\right|_{n_{\rm GS}} = \mu\,, \tag{2.25}$$

where the chemical potential μ was included to guarantee that the integral of the electron density $n(\mathbf{r})$ reproduces the number of electrons, N.

2.2.2 Kohn-Sham equations

The Hohenberg-Kohn theorem above states that the ground-state energy is a functional of the ground-state electron density and is minimized by $n_{\rm GS}$. However, the formal solution of the minimization task in Eq. (2.25) is not trivial. Kohn and Sham (`KS`) had the idea of splitting the unknown functional in Eq. (2.24), $F[n]$, as

$$F[n] = \underbrace{-\sum_i \int d\mathbf{r}\,\phi_i^*(\mathbf{r})\,\frac{\nabla^2}{2}\,\phi_i(\mathbf{r})}_{\text{kinetic term}} + \underbrace{\frac{1}{2}\iint d\mathbf{r}\,d\mathbf{r}'\,\frac{n(\mathbf{r})\,n(\mathbf{r}')}{|\mathbf{r}-\mathbf{r}'|}}_{\text{Hartree energy}} + \underbrace{E_{\rm xc}[n]}_{\text{xc energy}}\,. \tag{2.26}$$

This separation consists of a kinetic-energy term which is identical to the kinetic energy of a system of fictitious non-interacting electrons (`KS-electrons`) having the same ground-state electron density of the original electron system. In addition, Eq. (2.26) contains the Hartree energy, $E_{\rm H}[n]$, corresponding to the classical electrostatic energy of the electron charge density $n(\mathbf{r})$. Finally, they introduced an extra term, $E_{\rm xc}[n]$, contains everything that was not considered in the previous terms and is referred to as exchange-correlation energy. If $E_{\rm xc}[n]$ was known exactly, the ground-state energy could be determined using the electron density (see Section 2.2.3 for more details). Applying the minimization procedure, Eq. (2.25, and using the expression of $F[n]$ in Eq. (2.26), Kohn and Sham demonstrated that the exact ground-state electron density $n_{\rm GS}(\mathbf{r})$ can be expressed as

$$n_{\rm GS}(\mathbf{r}) = \sum_i^N |\phi_i(\mathbf{r})|^2\,, \tag{2.27}$$

where the single-particle wave functions ("orbitals") $\{\phi_i(\mathbf{r})\}$ are obtained from the solution of the `KS` equations

$$\hat{h}_{\texttt{KS}}\,\phi_i(\mathbf{r}) \equiv \left[-\frac{\nabla^2}{2} + v(\mathbf{r}) + v_{\rm H}(\mathbf{r},[n]) + v_{\rm xc}(\mathbf{r},[n])\right]\phi_i(\mathbf{r}) = \varepsilon_i\,\phi_i(\mathbf{r})\,. \tag{2.28}$$

Here, v is the external nuclear potential and $v_{\rm H}$ is the Hartree potential. The additional term, $v_{\rm xc}$, is the exchange-correlation potential and is given by:

$$v_{\rm xc}(\mathbf{r},[n]) = \left.\frac{\delta E_{\rm xc}[n]}{\delta n(\mathbf{r})}\right|_{n_{\rm GS}}\,. \tag{2.29}$$

2.2.3 Exchange-correlation functionals

In the previous section it was assumed that the exchange-correlation energy $E_{[}n]$ was known and the **KS** equations were solved, thus, the electron density could be determined. In practice, $E_{\mathrm{xc}}[n]$ is not known and approximations must be used. The two classes of approximations employed in this bachelor's thesis are presented below.

- The first class of approximations is based on the results for the uniform electron-gas model. This assumption provides exact results for the case of constant density and would be acceptable for slowly varying densities. This is not the case of the electron density in a solid, however, due to a cancellation of errors, this approximation, known as the local-density approximation (**LDA**) [6], provides quite good results for the structural and dynamical properties of solids.

- The second class of approximations for $E_{\mathrm{xc}}[n]$ utilizes the local gradient of the electron density in addition to the description of exchange and correlation given by the **LDA**. Approximations of this type are called generalized gradient approximations (**GGA**). There are many different ways in which the information about the gradient of the electron density can be incorporated into the **GGA** functional. There are therefore a large number of different **GGA** functionals. The best known are the Perdew-Wang functional (**PW91**) [6], the Perdew-Burke-Enzerhof functional (**PBE**) [6], and the PBE functional revised for solids (**PBEsol**) [9]. **PBEsol** was developed specifically for solids in order to increase the accuracy of the calculations.

2.2.4 Self-consistent calculations

We have seen in Section 2.2.2 that, after the **KS** equations have been solved, the ground-state electron density $n(\mathbf{r})$ (we have omitted the label **GS** for the sake of simplicity) can be determined. However, to solve these equations, the Hartree and the exchange-correlation potential have to be known, which themselves depend on the electron density. The following algorithm is used to solve this problem:

1. Define an initial electron density $n_0(\mathbf{r})$.

2. Solve the **KS** equations using the initial electron density $n_0(\mathbf{r})$.

3. Use the solution to calculate the electron density $n_{\mathrm{new}}(\mathbf{r})$ according to Eq. (2.27).

4. Compare the electron density $n_{\text{new}}(\mathbf{r})$ obtained with the initial electron density $n_0(\mathbf{r})$. When they are the same, then the ground-state electron density is found; if this is not the case, the initial electron density $n_0(\mathbf{r})$ must be adjusted. This procedure is repeated until the difference $n_0 - n_{\text{new}}$ fulfills some convergence criteria.

2.3 Density-functional perturbation theory

The density-functional perturbation theory (`DFPT`) was used to calculate the phonon-dispersion relations in this work. This is one of the linear-response techniques. These use the relationship between ionic displacements and the forces experienced by the other ions in the unit cell. In order to describe briefly the way in which `DFPT` works, we start from the `KS` equations written for a system which includes a general external perturbation (the label `KS` will be omitted in the following):[1]

$$\hat{h}\,\phi_{n\mathbf{k}}(\mathbf{r}) = \varepsilon_{n\mathbf{k}}\,\phi_{n\mathbf{k}}(\mathbf{r})\,. \tag{2.30}$$

The Hamiltonian $\hat{h}$ can be expanded up to the linear order in the perturbation $\delta\hat{h}$ as

$$\hat{h} = \hat{h}^{(0)} + \lambda\,\delta\hat{h} + O(\lambda^2)\,, \tag{2.31}$$

where $\hat{h}^{(0)}$ is the unperturbed Hamiltonian. Similar expansions to Eq. (2.31) hold for $\phi_{n\mathbf{k}}(\mathbf{r})$ and $\varepsilon_{n\mathbf{k}}$. Including these expansions in Eq. (2.30) yields

$$\begin{aligned}\Big[\hat{h}^{(0)} + \lambda\,\delta\hat{h} + \dots\Big]\Big[\phi^{(0)}_{n\mathbf{k}}(\mathbf{r}) + \lambda\,\delta\phi_{n\mathbf{k}}(\mathbf{r}) + \dots\Big] = \\ \Big[\varepsilon^{(0)}_{n\mathbf{k}} + \lambda\,\delta\varepsilon_{n\mathbf{k}} + \dots\Big]\Big[\phi^{(0)}_{n\mathbf{k}}(\mathbf{r}) + \lambda\,\delta\phi_{n\mathbf{k}}(\mathbf{r}) + \dots\Big]\,.\end{aligned} \tag{2.32}$$

From the linear terms in λ, the so-called Sternheimer equations are obtained:

$$\Big[\hat{h}^{(0)} - \varepsilon^{(0)}_{n\mathbf{k}}\Big]\delta\phi_{n\mathbf{k}}(\mathbf{r}) = -\Big[\delta\hat{h} - \delta\varepsilon_{n\mathbf{k}}\Big]\phi^{(0)}_{n\mathbf{k}}(\mathbf{r})\,. \tag{2.33}$$

The linear response of the wave function, $\delta\phi_{n\mathbf{k}}(\mathbf{r})$, can thus be determined by solving the linear system in Eq. (2.33). Since the Hamiltonian response depends implicitly on the wave function response via the density and potential response, the Sternheimer equations must be solved self-consistently:

$$\delta\phi_{n\mathbf{k}} \to \delta n(\mathbf{r}) \to \delta v_{\text{eff}}(\mathbf{r}) \to \delta\hat{\mathbf{h}} \to \delta\phi_{n\mathbf{k}}\,, \tag{2.34}$$

[1] From now on, we use explicitly the fact that the nuclear configuration has the periodicity of a crystal. Therefore, the index used in the `KS` equations must be written as $i \equiv (n, \mathbf{k})$, where n is the band index and $\mathbf{k}$ a vector in the first Brillouin zone of the crystal.

where $\delta v_{\text{eff}} = \delta v + \delta v_{\text{H}} + \delta v_{\text{xv}}$. When applying the density-functional perturbation theory to phonons, the external perturbation manifests itself in the form of a collective phonon-like displacement of the nuclei from their equilibrium position, $\boldsymbol{u}_{l\alpha}$:

$$\delta \to \delta^{\mathbf{q}}_{\alpha j} \quad : \quad \mathbf{X}^0_{l\alpha} \to \mathbf{X}^0_{l\alpha} + \boldsymbol{u}_{l\alpha} \equiv \mathbf{X}^0_{l\alpha} + \mathrm{e}^{\imath \mathbf{q}\cdot\mathbf{R}_l}\, \delta \boldsymbol{u}_{\alpha} \,, \tag{2.35}$$

where j is the index of the Cartesian component, $\mathbf{R}_l$ is the identifier for the unit cell, α labels the atom in the unit cell, $\mathbf{q}$ represents the phonon wave vector, and $\delta\boldsymbol{u}_\alpha$ is an infinitesimal displacement vector.

From the results of the converged solution of the Sternheimer equation for the density and potential response, the linear response of the atomic forces, $\delta^{\mathbf{q}}_{\alpha i} F_{\beta j}$, can be calculated in one step [15]. The linear response corresponds directly to the entries of the dynamical matrix:

$$\delta^{\mathbf{q}}_{\alpha i} F_{\beta j} = \sqrt{M_\alpha M_\beta}\, D^{\beta j}_{\alpha i}(\mathbf{q}) \,. \tag{2.36}$$

Once the dynamical matrix has been determined, the phonon frequencies $\omega_\nu(\mathbf{q})$ and the eigenvectors $\mathbf{w}_\nu(\mathbf{q})$ are obtained from the solution of the following eigenvalue problem:

$$\underline{\underline{\mathbf{D}}}(\mathbf{q}) \cdot \mathbf{w}_\nu(\mathbf{q}) = \omega^2_\nu(\mathbf{q})\, \mathbf{w}_\nu(\mathbf{q}) \,. \tag{2.37}$$

In general, and in this thesis, the calculations are performed on a grid of $\mathbf{q}$-points spanning the entire first Brillouin zone. Dynamical matrices can be interpolated on any points within this grid using discrete Fourier transforms [16].

2.3.1 Dynamical matrix of polar materials

Contrary to non-polar materials, in polar systems the effective long-range electrostatic interaction between the atoms makes the use of the direct interpolation described in the previous section inefficient. Furthermore, the dynamical matrix at the Γ point is non-analytical in this case, making the phonon frequencies at Γ to be dependent on the direction of $\mathbf{q}$ when approaching to Γ. These problems are solved by writing the dynamical matrix as the sum of an analytical short-range (`SR`) part (that can be interpolated efficiently by discrete Fourier transforms) and a long-range (`LR`) one (that can be calculated explicitly)

$$\underline{\underline{\mathbf{D}}}(\mathbf{q}) = \underline{\underline{\mathbf{D}}}_{\mathtt{SR}}(\mathbf{q}) + \underline{\underline{\mathbf{D}}}_{\mathtt{LR}}(\mathbf{q}) \,, \tag{2.38}$$

where the last term depends on the Born effective-charge tensor $\underline{\underline{\mathbf{Z}}}^*_\alpha$ and on the clamped-nuclei dielectric tensor $\underline{\underline{\boldsymbol{\epsilon}}}^\infty$. The Born effective charges are related to the

total (ionic+ electronic) macroscopic polarization $\mathbf{P}^{(\mathrm{tot})}$ induced by a phonon at the Γ point, calculated at zero macroscopic electric field, $\mathbf{E}^{\mathrm{mac}}$, [16]:

$$Z^*_{\alpha,ij} = \Omega\sqrt{M_\alpha}\ \frac{\partial P_i^{(\mathrm{tot})}}{\partial A_{\alpha j}}\bigg|_{\mathbf{E}^{\mathrm{mac}}=0} . \tag{2.39}$$

Similarly, the clamped-nuclei dielectric constant is obtained from the variation of $\mathbf{P}^{(\mathrm{tot})}$ with respect to the macroscopic electric field, $\mathbf{E}^{\mathrm{mac}}$,

$$\epsilon^{\infty}_{ij} = \delta_{ij} + 4\pi\ \frac{\partial P_i^{(\mathrm{tot})}}{\partial E_j^{\mathrm{mac}}}\bigg|_{\mathbf{E}^{\mathrm{mac}}=0} . \tag{2.40}$$

2.4 Numerical solution

Numerical approximations are needed to solve the Kohn-Sham and Sternheimer equations discussed in the previous sections. In practice, these approximations are achieved by expanding the `KS` orbitals in terms of a finite basis set.

In the following sections, we first describe how to transform the formal `KS` equations into matrix form. Then, we introduce the **`exciting`** code, which was used in this thesis to solve the matrix equivalent of the Kohn-Sham and Sternheimer equations.

2.4.1 Expansion into basis functions

For a numerical solution of the `KS` equations, the `KS` wave functions, $\phi_i(\mathbf{r})$ are expanded in terms of a finite basis set, $\{\varphi_\gamma(\mathbf{r})$; with $\gamma = 1, \ldots, \gamma_{\max}\}$:

$$\phi_i(\mathbf{r}) = \sum_{\gamma}^{\gamma_{\max}} c_{i\gamma}\, \varphi_\gamma(\mathbf{r}) . \tag{2.41}$$

If this result is combined with Eq. (2.28), a matrix (secular) equation for the unknown coefficients $c_{i\gamma}$ is obtained:

$$\sum_{\gamma}^{\gamma_{\max}} \Big[\underline{\underline{\mathbf{h}}} - \varepsilon_i\, \underline{\underline{\mathbf{S}}}\Big]_{\kappa\gamma} c_{i\gamma} = 0 , \tag{2.42}$$

where we introduced the Hamiltonian matrix in the atomic orbitals representation

$$\Big[\underline{\underline{\mathbf{h}}}\Big]_{\kappa\gamma} = \int d\mathbf{r}\, \varphi^*_\kappa(\mathbf{r})\, \hat{h}_{\mathtt{KS}}\, \varphi_\gamma(\mathbf{r}) \tag{2.43}$$

and the so-called overlap matrix

$$\left[\underline{\underline{\mathbf{S}}}\right]_{\kappa\gamma} = \int d\mathbf{r}\, \varphi^*_\kappa(\mathbf{r})\, \varphi_\gamma(\mathbf{r})\,. \tag{2.44}$$

Thus, the solution of the KS equations can be represented as the solution of the generalized eigenvalue problem in Eq. (2.42).

2.4.2 The software package exciting

The all-electron full-potential computer package **exciting** was used to calculate the total energies and the phonon-dispersion relations. In **exciting**, linearized augmented plane waves (**LAPW**s) and local orbitals (**lo**) are used as basis functions to solve the Kohn-Sham equations. In this section, we give first a short description of these basis functions following Refs. [7, 8]. Then, we give some more details about the role of symmetry in the solution of the Sternheimer equation in **exciting**.

Basis functions in exciting

The core idea behind the use of augmented plane waves (**APW**s) is to divide space into muffin-tin (MT) and interstitial (I) regions. The muffin-tin regions are spheres with radii $R_{\mathtt{MT}}$ with the atomic nuclei at their centers, whose positions are indicated by $\boldsymbol{\tau}_\alpha$. The muffin-tin regions do not intersect with each other. The remaining space is the interstitial region. The KS orbitals[2] are expanded with the aid of the augmented plane waves (**APW**s):

$$\phi_{n\mathbf{k}}(\mathbf{r}) = \sum_{\mathbf{G}} c^{\mathbf{k}}_{n\mathbf{G}}\, \varphi^{\mathtt{APW}}_{\mathbf{G}+\mathbf{k}}(\mathbf{r})\,. \tag{2.45}$$

Here, the sum runs over the reciprocal-lattice vectors $\mathbf{G}$. The APW basis functions are formed as follows:

$$\varphi^{\mathtt{APW}}_{\mathbf{G}+\mathbf{k}}(\mathbf{r}) = \begin{cases} \sum_{lm} A^{\mathbf{G}+\mathbf{k}}_{lm\alpha}\, w_{l\alpha}(r_\alpha)\, Y_{lm}(\hat{\mathbf{r}}_\alpha)\,, & r_\alpha \le R_{\mathrm{MT}} \\ \frac{1}{\sqrt{\Omega}}\, \mathrm{e}^{\imath(\mathbf{G}+\mathbf{k})\cdot\mathbf{r}}, & \mathbf{r} \in \mathtt{I}\,. \end{cases}, \tag{2.46}$$

where $\mathbf{r}_\alpha = \mathbf{r} - \boldsymbol{\tau}_\alpha$ and Ω represents the volume of the unit cell. The muffin-tin region part of the **APW**s is expanded in the form of spherical harmonics $Y_{lm}(\hat{\mathbf{r}}_\alpha)$ and radial functions $w_{l\alpha}(r_\alpha)$. The coefficients $A^{\mathbf{G}+\mathbf{k}}_{lm\alpha}$ make the **APW**s continuous at the sphere boundary.

As an alternative to the **APW**s just described, linearized augmented plane waves (**LAPW**s) can also be used as a basis. The LAPW basis function within the muffin-tin

[2] Here, the index $i = (n, \mathbf{k})$ for periodic crystals.

region around $\boldsymbol{\tau}_\alpha$ is given by:

$$\varphi^{\texttt{LAPW}}_{\mathbf{G+k}}(\mathbf{r}) = \sum_{lm} \left[A^{\mathbf{G+k}}_{lm\alpha}\, w_{l\alpha}(r_\alpha;\epsilon_{l\alpha}) + B^{\mathbf{G+k}}_{lm\alpha}\, \dot{w}_{l\alpha}(r_\alpha;\epsilon_{l\alpha}) \right], \tag{2.47}$$

where $\epsilon_{l\alpha}$ are the energy parameters. In Eq. (2.47), $A^{\mathbf{G+k}}_{lm\alpha}$ and $B^{\mathbf{G+k}}_{lm\alpha}$ are coefficients that ensure the continuity of the **LAPW** and its spatial derivatives at the boundaries of the **MT**s.

In addition to the **APW**s and **LAPW**s, in **exciting** local orbitals (**lo**) can be considered as further basis functions. These functions are strictly non-zero within the muffin-tin regions and must vanish at the **MT** boundaries.

In the most general case, the **KS** orbitals can be represented in **exciting** as the sum of the **APW**s or **LAPW**s and **lo**s contributions:

$$\phi_{n\mathbf{k}}(\mathbf{r}) = \sum_{\mathbf{G}} c^{\mathbf{k}}_{n\mathbf{G}}\, \varphi^{\texttt{APW/LAPW}}_{\mathbf{G+k}}(\mathbf{r}) + \sum_{\mu} c^{\mathbf{k}}_{n\mu}\, \varphi^{\texttt{lo}}_{\mu}(\mathbf{r})\,. \tag{2.48}$$

By reducing the muffin-tin radius $R_{\texttt{MT}}$ more plane waves are needed to appropriately describe the **KS** wave functions in the interstitial region. Therefore, a useful parameter that describes the size of the basis set is the product $R^{\min}_{\texttt{MT}}\,|\mathbf{G}+\mathbf{k}|_{\max}$, where $R^{\min}_{\texttt{MT}}$ stands for the minimum **MT** radius in the unit cell and $|\mathbf{G}+\mathbf{k}|_{\max}$ is the maximum cut-off value that limits the allowed values of $\mathbf{G}$.

Role of symmetry in the solution of the Sternheimer equation

When solving the Sternheimer equation, the **DFPT** implementation in **exciting** exploits carefully the symmetry of the phonon perturbation. Indeed, not every atom has to be displaced individually in the three Cartesian directions. Special symmetry-adapted displacement patterns (irreducible representations, in **exciting**: **irreps**) can be used:

$$\delta^{\mathbf{q}}_{I\varrho} = \sum_{l,\alpha} p^{I\varrho}_{l\alpha}(\mathbf{q})\, \delta^{\mathbf{q}}_{l\alpha}\,, \tag{2.49}$$

where I denotes the displacement pattern for a given $\mathbf{q}$ and ϱ denotes the so-called member of the displacement pattern.

Chapter 3

Results

In this chapter, the results of the calculations carried out for germanium and lithium fluoride are presented and discussed. The computational details for the calculations are described first. This is followed by an examination of the optimization of the equilibrium configuration required to determine the phonon properties. Finally, the phonon-dispersion relations and phonon density of states for Ge and LiF are presented, examined, and compared with experimental and theoretical values from the literature.

3.1 Computational details

The calculations of the lattice dynamics of germanium and lithium fluoride were all carried out using **DFT** and **DFPT** implemented in the **exciting** code. For the discussion of the results and in particular for the comparison with other theoretically and experimentally determined results, the local-density approximation **LDA** [6] and the two generalized gradient approximations, **PBE** [6] and **PBEsol** [9], were used for the exchange-correlation functional.

The basis functions in the muffin-tin regions were adapted for each element. In **exciting**, this is done by modifying the **species** files belonging to each element. The files used for the elements Ge, Li, and F [17] can be found in Appendix A.

When using the **exciting** code, there is a large number of parameters [18, 19, 20] that determine the accuracy of the target variable(s) of a calculation. By varying these, the required precision of the target variable(s) can be achieved, whereby greater precision is usually accompanied by higher computational costs. The parameters that are particularly important for this work are briefly explained in the following.

```
<input>

   <title>Germanium</title>

   <structure speciespath="$EXCITINGROOT/species">

      <crystal scale="10.715">
         <basevect> 0.5     0.5     0.0 </basevect>
         <basevect> 0.5     0.0     0.5 </basevect>
         <basevect> 0.0     0.5     0.5 </basevect>
      </crystal>

      <species speciesfile="Ge.xml">
         <atom coord="0.00 0.00 0.00" />
         <atom coord="0.25 0.25 0.25" />
      </species>

   </structure>

   <groundstate
      ngridk="24 24 24"
      swidth="0.01"
      rgkmax="6"
      gmaxvr="18"
      xctype="LDA_PW">
   </groundstate>

</input>
```

Figure 3.1: Example of the **exciting** input file for the calculation of the ground state of Ge with **LDA**.

- The number of **k**-points along the basis vector directions for the numerical integration is given by a set of three integers and denoted by **ngridk**.
- The parameter **rgkmax** determines the size of the basis set and results from the product $R_{\mathrm{MT}}^{\mathrm{min}} |\mathbf{G} + \mathbf{k}|_{\mathrm{max}}$ (see Section 2.4.2).
- The maximum length of the reciprocal lattice vector for expanding the interstitial density and potential is determined by **gmaxvr**.
- The parameter **swidth** is relevant for metallic systems. It describes the width of a smearing function, which is necessary to calculate the occupancies of the Kohn-Sham states.
- Finally, the parameter **ngridq** should be mentioned, which is expressed by a set of three integers and describes the number of **q**-points along the basis vector directions in reciprocal space.

An example of the input file for a ground-state calculation can be seen in Fig. 3.1.

Table 3.1: Abbreviated denominations used in this thesis for the most important computational parameters for a calculation.

parameter in **exciting**	short cut
ngridk	**k**
rgkmax	**r**
gmaxvr	**g**
swidth	**s**
ngridq	**q**

In this work, abbreviated denominations are used to describe the parameters of a calculation in order to ensure simplicity. The abbreviated denominations are shown in Table 3.1. For example, the label **4q.16k.8r.40g** means that a calculation was carried out with **ngridq**=4×4×4, **nrgidk**=16×16×16, **rgkmax**=8, and **gmaxvr**=40.

3.2 Structure optimization

The calculation of the phonon properties first requires the determination of the equilibrium configuration of the crystal [21]. Since the materials investigated in this work, germanium and lithium fluoride, have cubic symmetry, it is sufficient to minimize the total energy of these systems as a function of the cubic lattice constant a to determine the equilibrium configuration. The starting point for the calculation is an initial guess for the lattice parameter. Then, the total energy is calculated for different shifts of the lattice parameter in negative and positive direction. The pairs of volumes determined from the lattice parameters ($\Omega = a^3/4$) and the corresponding energies are fitted using the Birch-Murnagham equation-of-state [22]:

$$E(\Omega) = E_0 + \frac{9\Omega_0 B_0}{16}\left\{\left[\left(\frac{\Omega_0}{\Omega}\right)^{\frac{2}{3}} - 1\right]^3 B_0' + \left[\left(\frac{\Omega_0}{\Omega}\right)^{\frac{2}{3}} - 1\right]^2 \left[6 - 4\left(\frac{\Omega_0}{\Omega}\right)^{\frac{2}{3}} - 1\right]\right\}, \tag{3.1}$$

with Ω_0 for the unit-cell volume at the energy minimum E_0, B_0 for the bulk modulus, and B_0' for the pressure derivative of the bulk modulus. The volume associated with the smallest energy can be determined from the fit and thus also the corresponding lattice parameter. Figure 3.2 visualizes a sample calculation of the optimal volume for Ge. All calculations performed in this work for Ge were carried out with the parameter **swidth**=0.01, due to its semimetal nature (see Section 3.1).

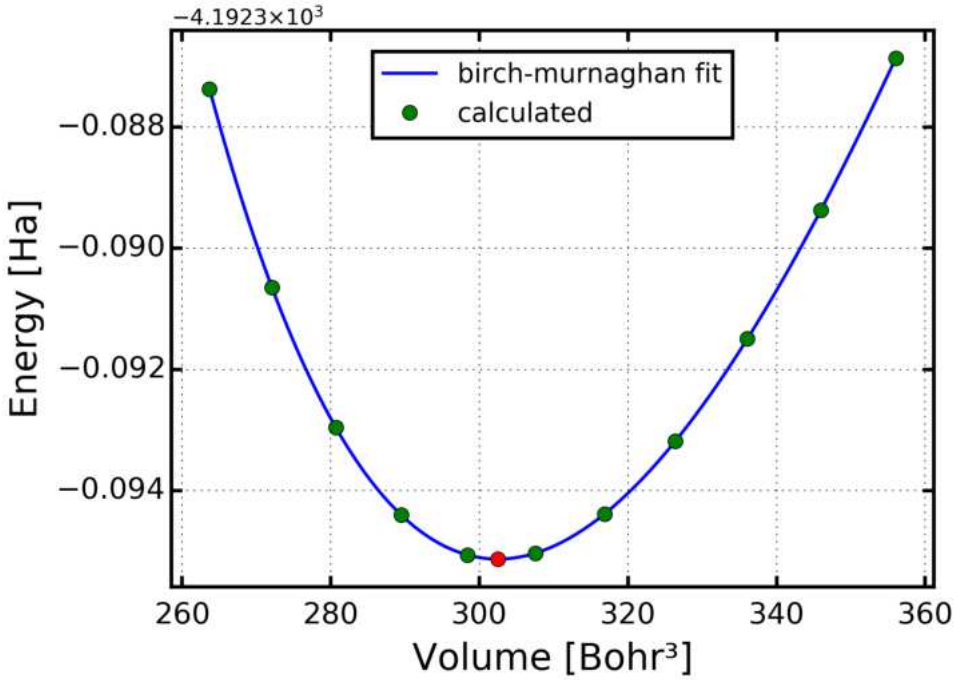

Figure 3.2: Determination of the lowest energy as a function of the volume for germanium by a fit using the Birch-Murnagham equation-of-state.

In order to guarantee the convergence criterion of three decimal digits for the lattice parameter a_0 in [Å], calculations were performed for both materials and all considered exchange-correlation functionals with different sets of computational parameters. The results of this analysis for Ge (LiF) are shown in Table 3.2 (3.3) for `LDA`. For the other `GGA` functionals, we get the same convergence behaviour. The converged lattice parameters and reference values from the literature for Ge and LiF are listed in the Tables 3.4 and 3.5, respectively.

3.3 Phonon properties

The density-functional perturbation theory (`DFPT`) (see Section 2.3), implemented in the `exciting` code, was used to calculate the phonon frequencies and create the phonon-dispersion relations as well as the phonon density of states for Ge and LiF. In order to achieve greater comparability, all calculations were carried out with the exchange-correlation functionals `LDA`, `PBE`, and `PBEsol`. The results of the calculations for Ge and LiF are presented and discussed in the next two sections for the relevant cases. An overview of the converged phonon properties calculated in this thesis can be found in Appendix B and C for Ge and LiF, respectively.

Table 3.2: Convergence of B_0, B_0', and a_0 in dependence of the values of **ngridk** and **rgkmax** for Ge calculated with **LDA**.

Ge	**ngridk**	8×8×8	12×12×12	16×16×16	20×20×20	24×24×24
	rgkmax					
	8	69.53	70.00	70.29	70.64	70.59
B_0 [GPa]	9	69.68	69.82	70.18	70.37	70.39
	10	69.61	69.75	70.14	70.33	70.33
	8	4.79	4.79	4.76	4.87	4.82
B_0'	9	4.99	4.84	4.77	4.79	4.82
	10	5.03	4.87	4.79	4.81	4.83
	8	5.6347	5.6359	5.6359	5.6351	5.6352
a_0 [Å]	9	5.6363	5.6385	5.6387	5.6389	5.6380
	10	5.6368	5.6390	5.6392	5.6389	5.6386

Table 3.3: Same as Table 3.2 for LiF.

LiF	**ngridk**	4×4×4	8×8×8	12×12×12	16×16×16	20×20×20
	rgkmax					
	7	76.48	87.41	86.19	86.53	86.32
B_0 [GPa]	8	86.28	86.38	86.43	86.47	87.28
	9	86.49	86.52	86.49	86.51	86.52
	7	2.74	4.49	4.27	4.32	4.28
B_0'	8	4.25	4.25	4.26	4.26	4.49
	9	4.28	4.27	4.27	4.27	4.27
	7	3.9067	3.9078	3.9078	3.9080	3.9079
a_0 [Å]	8	3.9115	3.9106	3.9105	3.9105	3.9079
	9	3.9117	3.9108	3.9108	3.9108	3.9108

Table 3.4: Equilibrium lattice constant a_0 of germanium.

Ge	Ref.	E_{xc}	a_0 [Å]
Present work		`LDA`	5.639
		`PBEsol`	5.692
		`PBE`	5.778
Theory	[23]	`LDA`	5.567
	[24]	`LDA`	5.625
	[25]	`PBEsol`	5.679
	[26]	`PBEsol`	5.675
	[25]	`PBE`	5.764
	[27]	`PBE`	5.78
Experiment	[28]		5.658
	[29]		5.658

Table 3.5: Same as Table 3.4 for lithium fluoride.

LiF	Ref.	E_{xc}	a_0 [Å]
Present work		`LDA`	3.911
		`PBEsol`	4.006
		`PBE`	4.067
Theory	[30]	`LDA`	3.886
	[26]	`LDA`	3.913
	[25]	`PBEsol`	4.005
	[26]	`PBEsol`	4.003
	[25]	`PBE`	4.064
	[26]	`PBE`	4.062
Experiment	[31]		4.026
	[32]		4.020

3.3.1 Germanium

In this section, the convergence behavior for the phonon-dispersion relations (PDR) and the phonon density of states (PDOS) is considered first, as well as the effects of different exchange-correlation functionals on the calculations. In addition, the results are compared with the results of Refs. [16] and [33]. Finally, problems occurring in the calculations are discussed and possible solutions are presented.

All calculations were carried out using 8r.18g and 0.01s, as these proved to be stable values for the structural optimization of Ge. For LDA, PBE, and PBEsol, calculations were carried out with both 4q and 8q as well as 8k, 16k, and 24k. In the following, the calculations performed with LDA are taken as a reference. This choice is also supported by the fact that LDA, for Ge, leads to phonon results that are the closest to experiment. Furthermore, for all our calculations, the convergence behaviour is the same, independently of the choice for the exchange-correlation functional.

First of all, we analyzed the convergence of the phonon properties with respect to the phonon **q**-grids. Figure 3.3 shows the results for the phonon frequencies and density of states corresponding to 4q.16k and 8q.16k. For Ge in the diamond structure, with two atoms in the basis, three acoustic and three optical modes are present (see Section 2.1.5). More precisely, there is one longitudinal-acoustic mode (LA), two transverse-acoustic modes (TA), one longitudinal-optical mode (LO) and two transverse-optical modes (TO). The analysis of Fig. 3.3 makes clear that the calculation with 4q is not satisfactory, in particular in the region in reciprocal space close to the K point. We conclude that the 8q mesh is necessary to show the correct details of the phonon-dispersion relations. The use of finer **q**-grids in non-polar materials, such as Germanium, does not improve appreciably the results. This is due to the short-range nature of the effective inter-atomic force constants in this kind of materials.

Then, we investigated the effect of the choice for the electronic **k**-grids. Figure 3.4 shows the PDR calculated with 8q.8k, 8q.16k, and 8q.24k. The only relevant differences among the PDR can be found for the 8q.8k calculation for the optical branches in the vicinity of the Γ point and for the LO at the L point (see the details in the lower panel of Fig. 3.4). Therefore, we assume the 8q.16k calculations to be converged (to the accuracy of less than 1 cm^{-1}).

Figure 3.5 shows a comparison of the LDA optical PDR calculated using the DFPT implementation of exciting with the full PDR from Ref. [16]. Although the general agreement between the two calculations is quite good, the exciting one is characterized by an untypical enhancement of the phonon frequencies close to the Γ point.

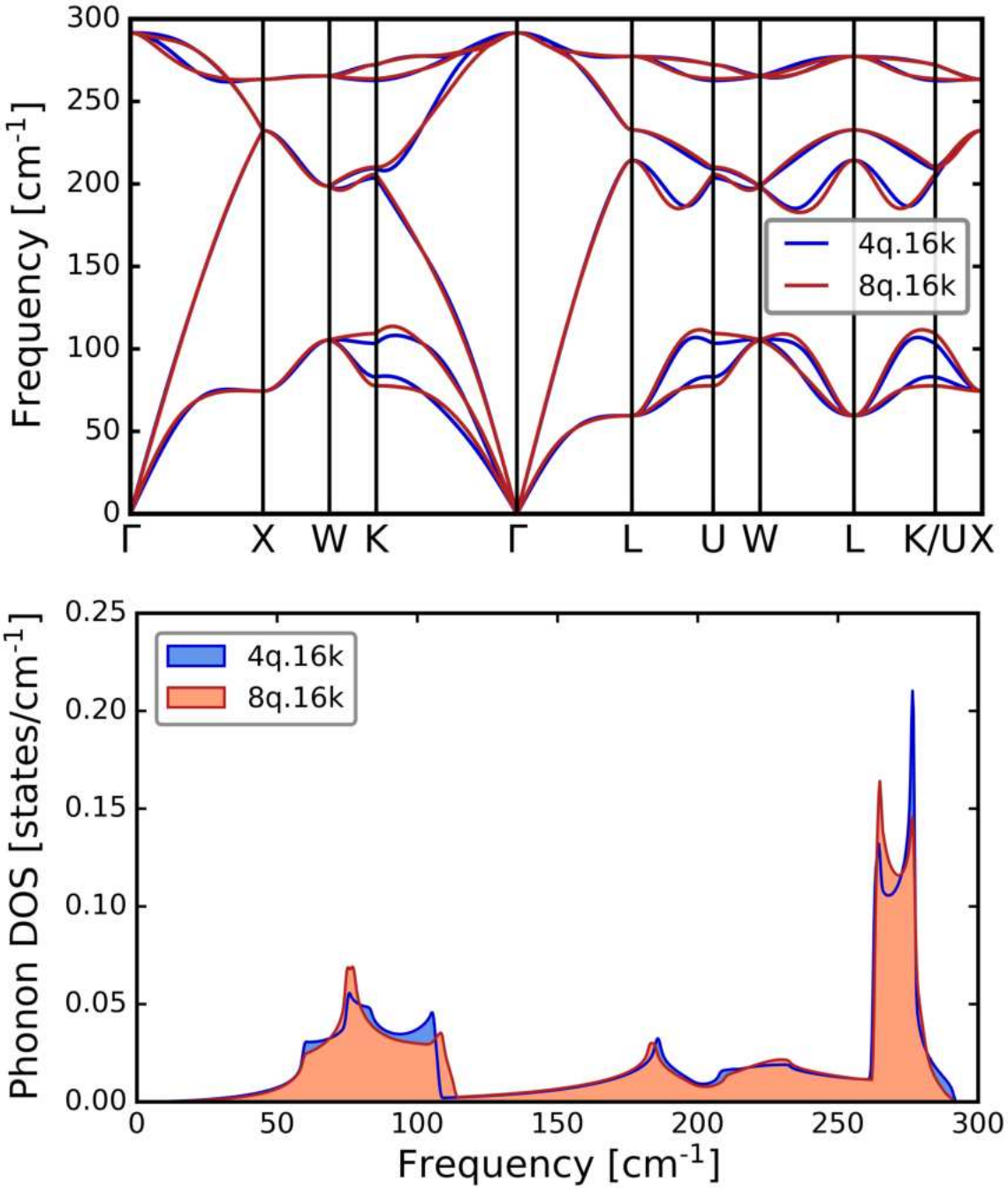

Figure 3.3: Comparison of the `LDA` phonon calculations for Ge. Upper panel: Phonon-dispersion relations for `4q.16k` (blue lines) and `8q.16k` (red lines). Lower panel: Phonon density of states.

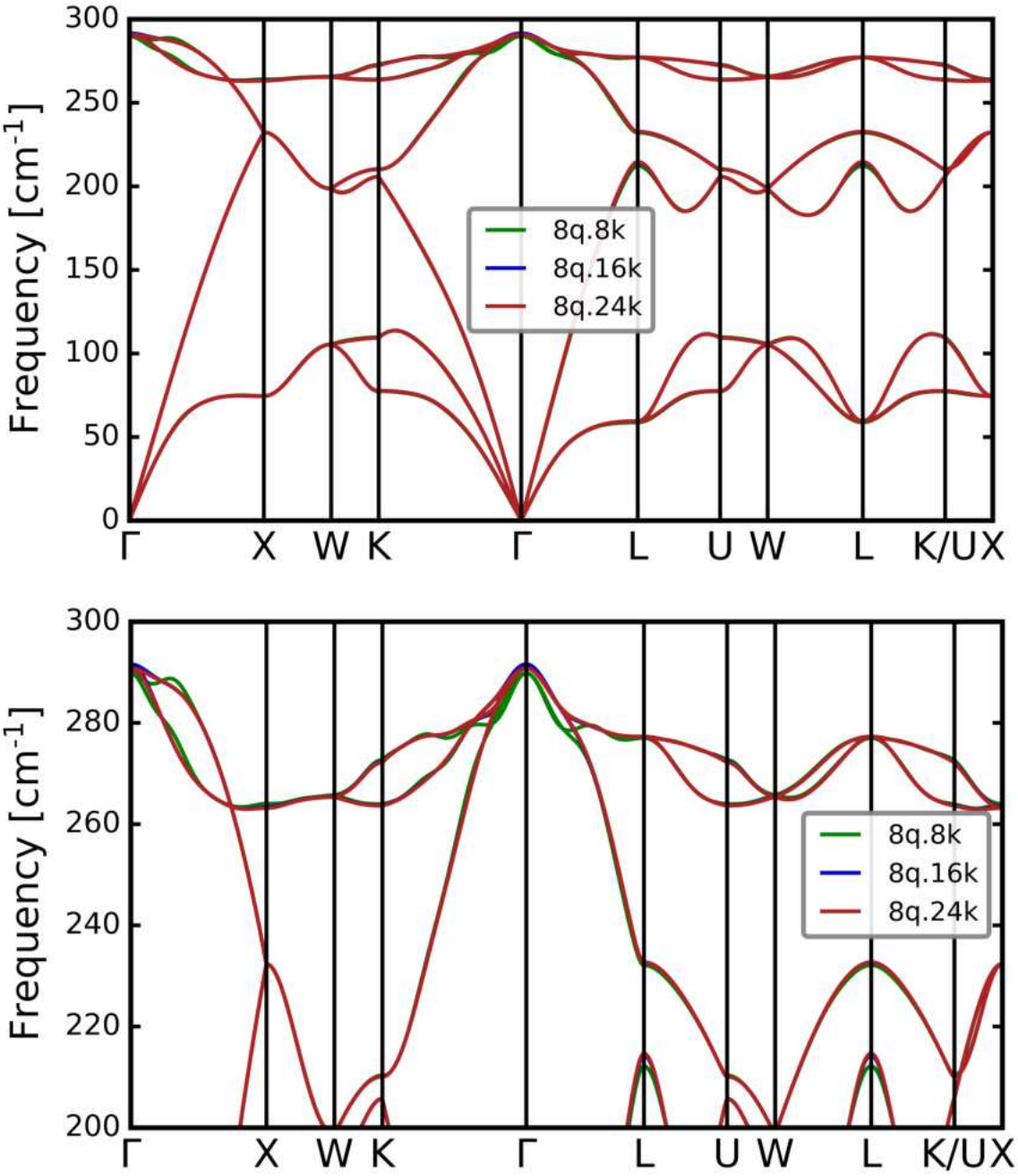

Figure 3.4: Comparison of the `LDA` phonon calculations for Ge. Upper panel: Phonon-dispersion relation for `8q.8k` (green lines), `8q.16k` (blue lines), and `8q.24k` (red lines). Lower panel: Same as upper panel in the frequency region between 250 and 300 cm^{-1}.

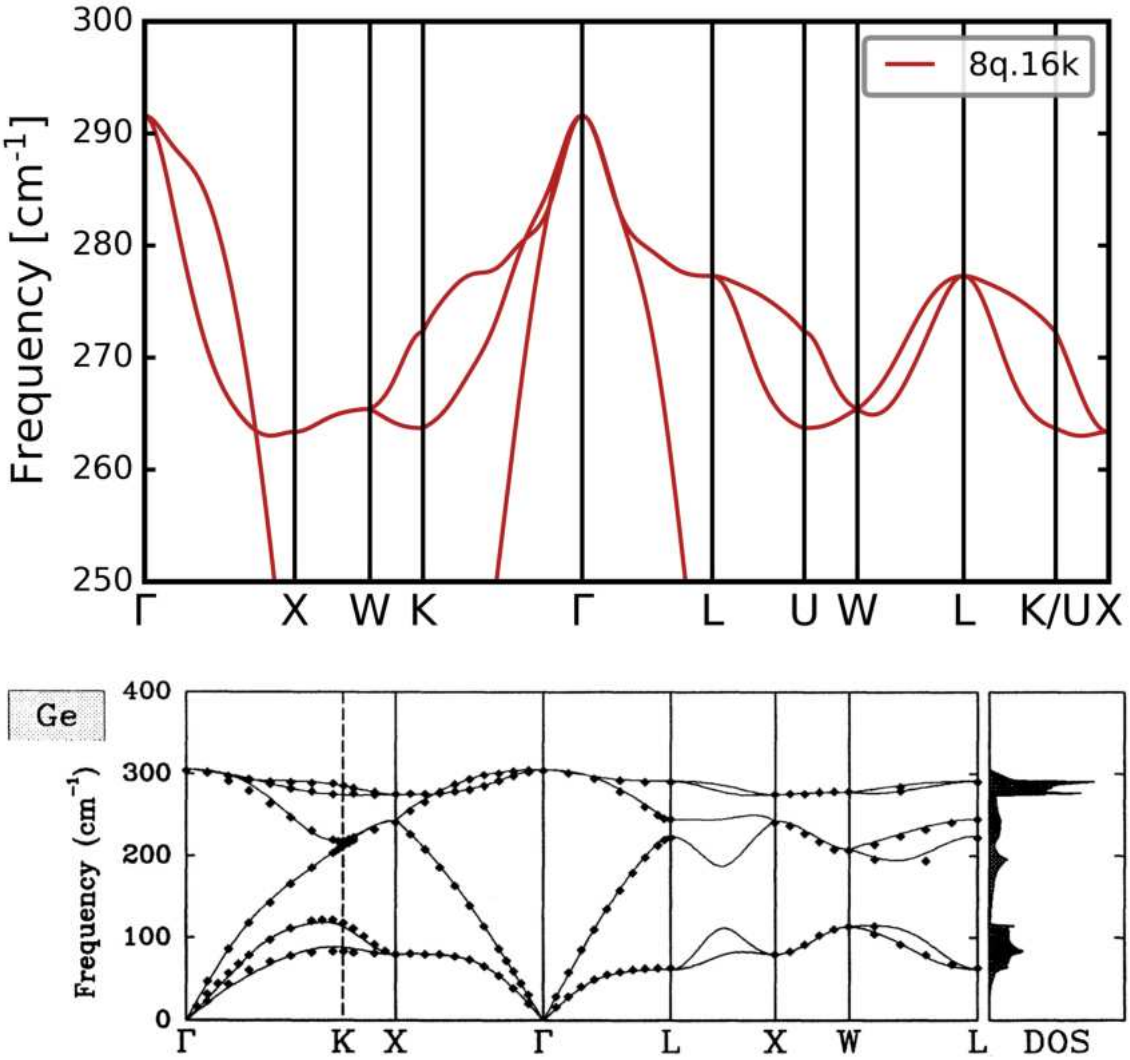

Figure 3.5: Phonon-dispersion relations calculated for Ge using `LDA`. Upper panel: Behaviour of the phonon-dispersion relations for `8q.16k` in the optical frequency region and. Lower panel: Phonon-dispersion relations from Ref. [16].

In order to investigate the origin of this discrepancy, we performed further calculations of the `LDA` phonon frequencies using the super-cell (`sc`) method in `exciting`. The results reported in Table 3.6 show that for the high-symmetry points X and L there is no difference between `DFPT` and `sc` calculations. At variance with this, the frequency of the `DFPT` optical phonons at Γ is shifted upwards with respect to the `sc` value of about $5\,\mathrm{cm}^{-1}$. This seems to indicate that there could be some issue with the implementation of `DFPT` in `exciting` at $\mathbf{q} = 0$.

Table 3.6: Comparison of the calculated and experimental phonon frequencies of Ge, in units of cm^{-1}, for the high-symmetry points Γ, X, and L of the first Brillouin zone.

	LDA				PBEsol	PBE	Expt.
	DFPT	sc	DFPT+Γ-sc	Ref. [16]	DFPT+Γ-sc	DFPT+Γ-sc	Ref. [33]
Γ_{Opt}	292	287	287	306	281	270	304
X_{TA}	74	74	74	80	72	75	80
X_{LA}	232	232	232	243	228	220	241
X_{TO}	263	263	263	275	258	246	276
X_{LO}	232	232	243	243	228	220	241
L_{TA}	59	59	59	62	58	60	63
L_{LA}	214	214	214	224	210	205	222
L_{TO}	277	277	277	291	272	260	290
L_{LO}	233	233	233	245	228	216	245

The full **sc** calculation of the **PDR** on a finer **q**-mesh is computationally very demanding and out of the purposes of this work. Therefore, we consider in this work as converged calculation the **DFPT** one with the dynamical matrix at Γ replaced by the one obtained with the **sc** method. The full **PDR** and **PDOS** can be obtained through interpolation. In the following, we denote this approach with the label "**DFPT**+Γ-**sc**". The results obtained in this way for **LDA** are shown in Fig. 3.6.

The correction procedure discussed above, was applied to the calculations for the other exchange-correlation functionals, **PBE** and **PBEsol**. Figure 3.7 shows a summary of the results produced in this way. The **PDR** and **PDOS** calculated with **LDA**, **PBEsol**, and **PBE** are qualitatively very similar, as can be seen from Fig. 3.7. However, it is noticeable that the curves for different exchange-correlation functionals are shifted against each other. For a fixed **k**-vector, the phonon frequencies for **LDA** are the highest and the ones for **PBE** are the lowest. The frequencies for **PBEsol** lie between those of **LDA** and **PBE**. This behaviour can be easily understood by considering the sequence of the corresponding equilibrium unit-cell volumes: $\Omega_{\mathtt{LDA}} < \Omega_{\mathtt{PBEsol}} < \Omega_{\mathtt{PBE}}$. Indeed, a smaller equilibrium volume leads to stronger effective interactions among the atoms and in turn to higher phonon frequencies. This trend becomes particularly clear if one looks at the values of the phonon frequencies at the high-symmetry points Γ, X, and L in Table. 3.6. Noticeable, there are also exceptions. The phonon frequencies of the **TA** modes deviate from this trend at the L and X points [16].

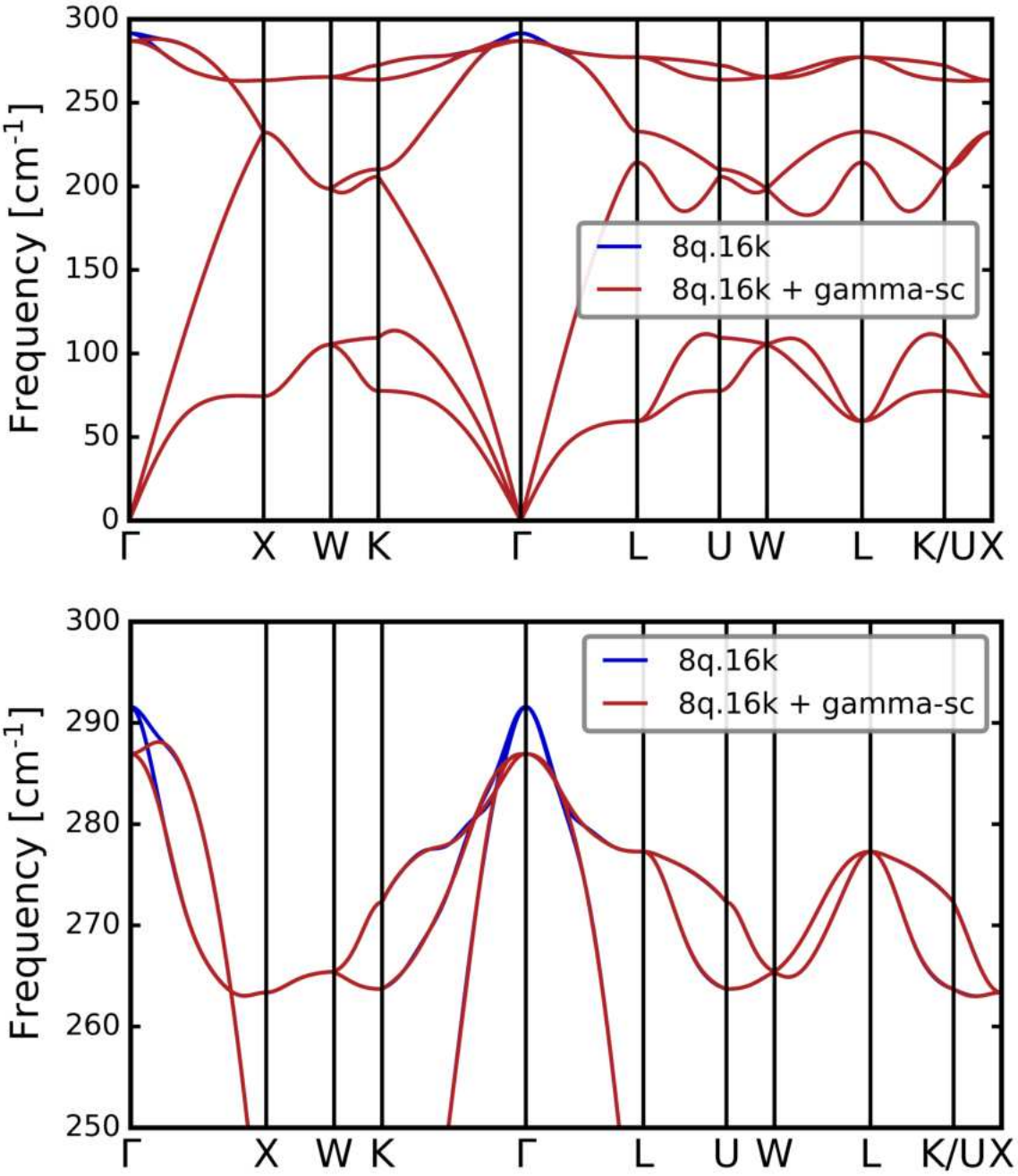

Figure 3.6: Phonon-dispersion relations of Ge for `LDA` obtained using the `DFPT`+Γ-`sc` approach (see the text for details). Upper panel: Phonon-dispersion relations in the full frequency range for `8q.16k` (blue lines) and `8q.16k`+Γ-`sc` (red lines). Lower panel: Same as the upper panel for phonon frequencies in the range between 250 and 300 cm^{-1}.

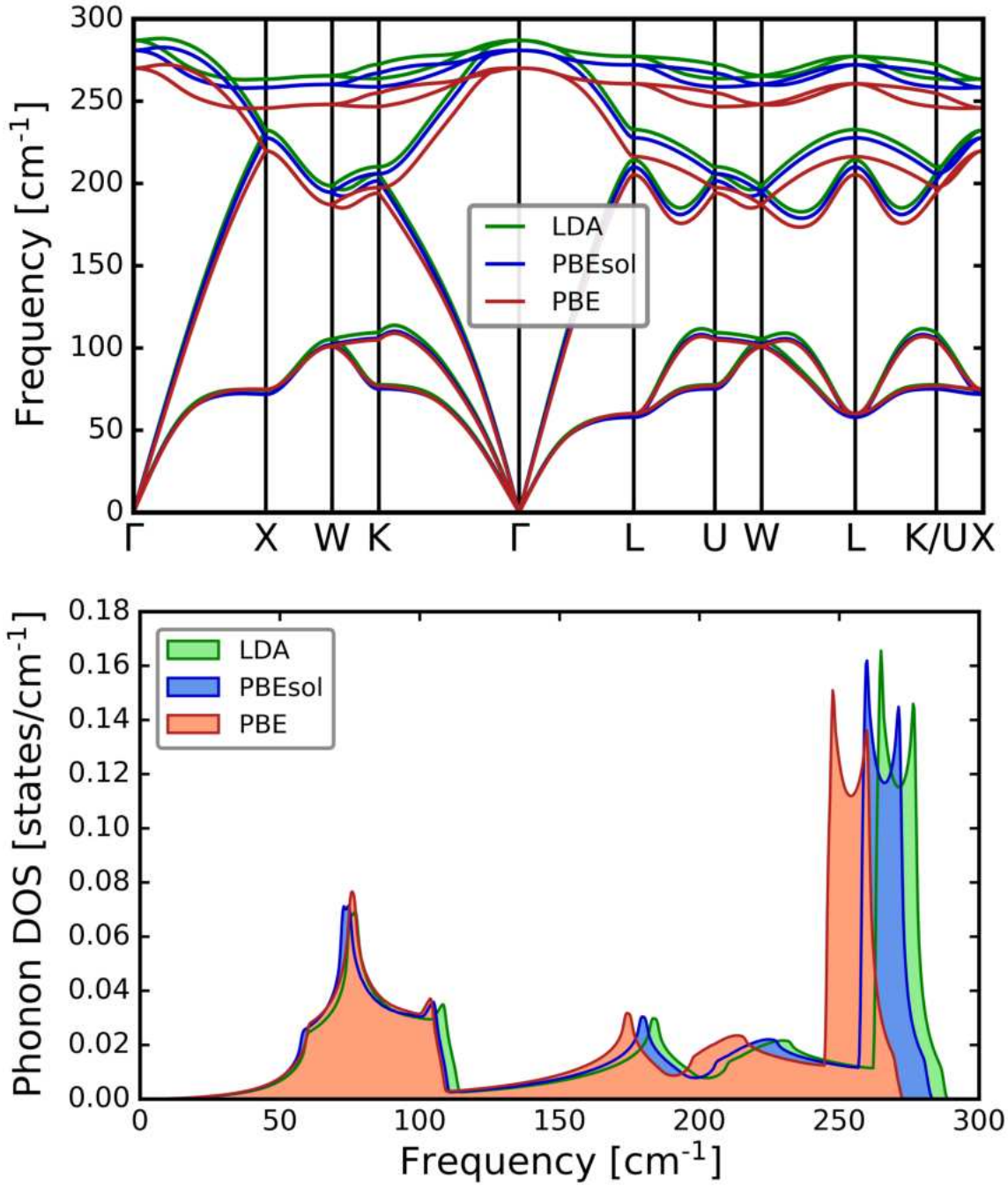

Figure 3.7: Comparison of the phonon calculations for Ge using `8q.16k` and the `DFPT`+Γ-`sc` approach (see the text for details). Upper panel: Phonon-dispersion relations obtained for `LDA` (green lines), `PBEsol` (blue lines), and `PBE` (red lines). Lower panel: Phonon density of states.

3.3.2 Lithium fluoride

In this section, we present and discuss the convergence behaviour of the phonon properties of lithium fluoride. All calculations were carried out using `8r` and `0.0001s`, as these proved to be stable values for the structural optimization of LiF. For `LDA`, `PBE`, and `PBEsol`, calculations were carried out with both `4q` and `8q` as well as `8k` and `16k`. In the following, the calculations performed with `PBEsol` are taken as a reference, as this choice leads to the closest phonon results to the experiment of Ref. [34]. Furthermore, for all our calculations, the convergence behaviour is mostly same, independently of the choice for the exchange-correlation functional. Deviations from the previous statement are considered explicitly in the following.

First of all, we analyzed the convergence of the phonon properties with respect to the phonon **q**-grids. Figure 3.8 shows the results for the phonon frequencies and density of states corresponding to `4q.16k.40g` and `8q.16k.40g`. Similarly to the case of Ge, we conclude that the `8q` mesh is enough to describe the `PDR` and `PDOS` of LiF. Even if LiF is a polar material with long-range effective electrostatic interactions between the atoms, the effect connected to these interactions is fully contained in the long-range part of the dynamical matrix, see Eqs. (2.38). This part can be treated exactly [16] in terms of an analytical expression depending on the Born effective charges and the clamped-nuclei dielectric constant.[1]

Then, we investigated the effect of the choice for the electronic **k**-grids. Figure 3.9 shows the `PDR` and `PDOS` calculated with `8q.8k.40g` and `8q.16k.40g`. The two `PDR` are practically indistinguishable, the only minor difference can be seen in the `PDOS` around 640 cm^{-1}. This deviation can be ascribed to the fact that the clamped-nuclei dielectric constant notoriously requires very fine **k**-grids to be considered converged.

An important test for LiF was the choice of the appropriate value for the parameter `gmaxvr`. While the value of `18g` was enough for ensure a convergence of the phonon frequencies of LiF for the `LDA` exchange-correlation functional, this value was not sufficient for the `GGA` functionals, as can be seen in Fig. 3.10. Indeed, for `PBEsol` and `PBE` a value of at least `40g` had to be chosen in order to ensure convergence of the phonon frequencies of LiF below 1 cm^{-1}. The difference between the results corresponding to `18g` and `40g` in Fig. 3.10 is directly visible, particularly (drastically) for the `PBE` calculations. This fact can be explained by considering that the `GGA` functionals depend on the numerical gradient of the electron density. In those regions of the unit cell where the density is very low, the numerical calculation of its gradient can be problematic due to the approximate description of the density.

[1] Due to the cubic symmetry of LiF, both the Born effective-charges tensors and the clamped-nuclei dielectric tensor, defined in Eqs. (2.39) and (2.40), respectively, have diagonal form.

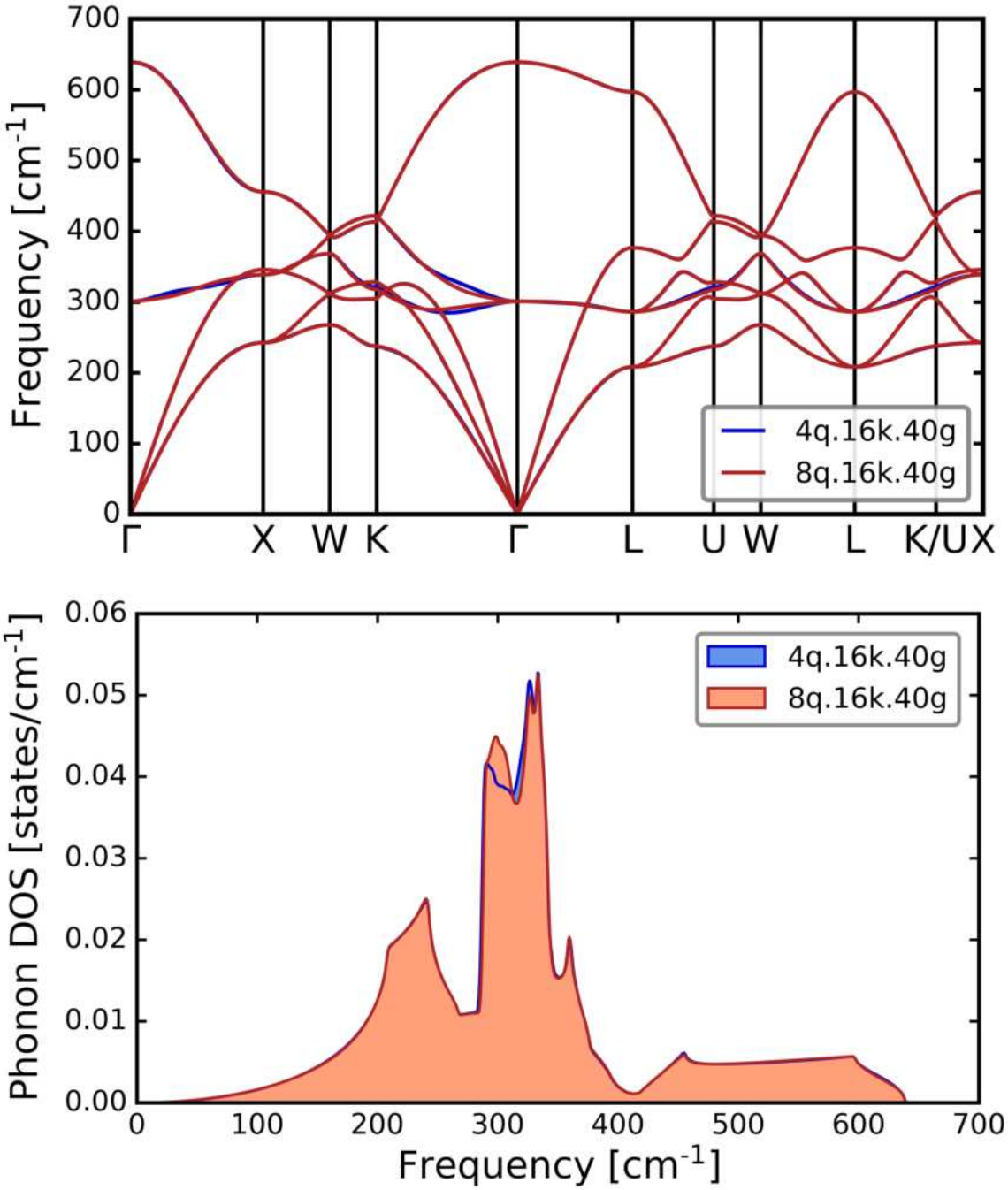

Figure 3.8: Comparison of the phonon calculations for LiF using `PBEsol`. Upper panel: Phonon-dispersion relations obtained with `4q.16k.40g` (blue lines) and `8q.16k.40g` (red lines). Lower panel: Phonon density of states.

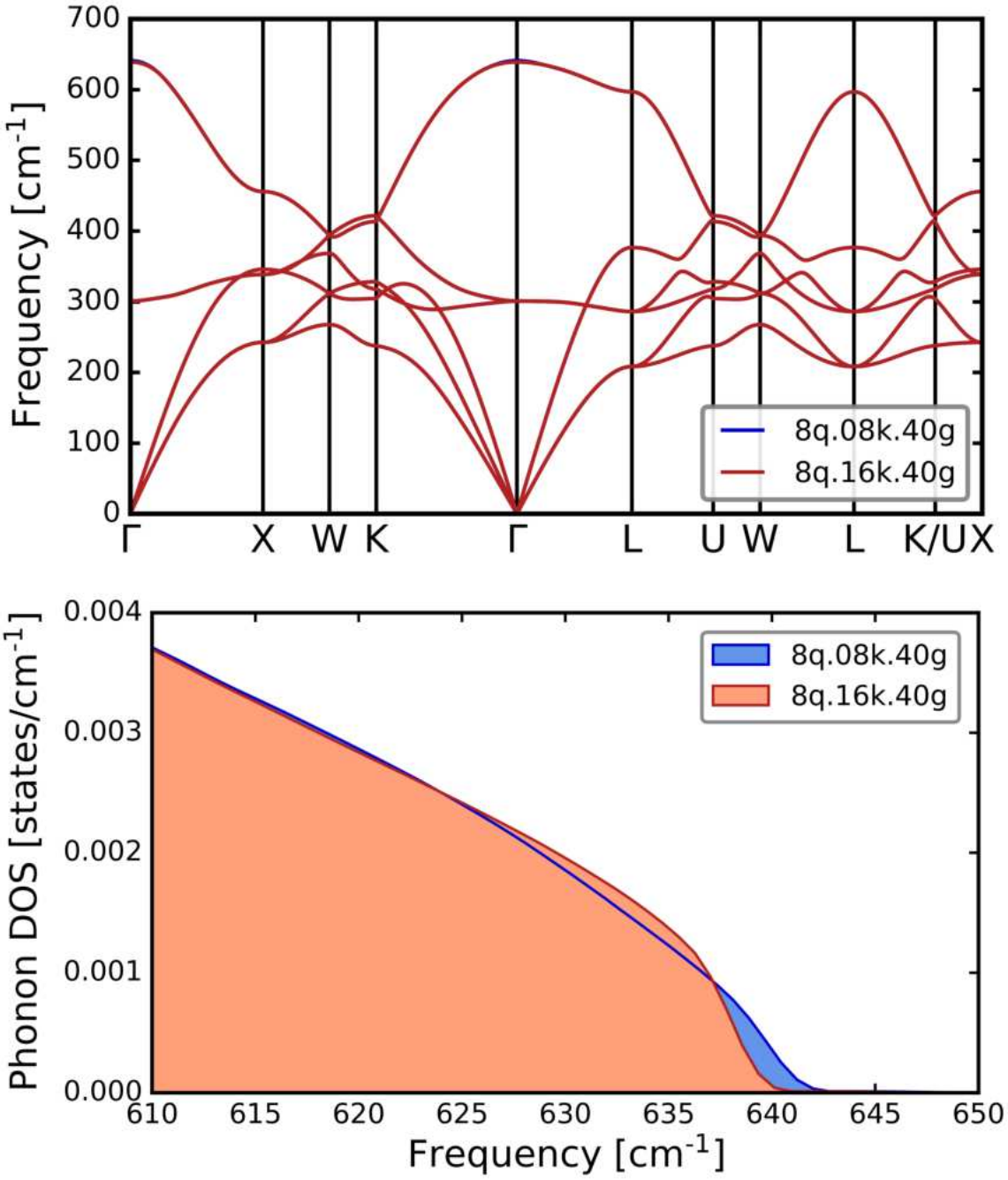

Figure 3.9: Comparison of the phonon calculations for LiF using `PBEsol`. Upper panel: Phonon-dispersion relations obtained with `8q.8k.40g` (blue lines) and `8q.16k.40g` (red lines). Lower panel: Phonon density of states in the frequency region between 610 and 650 cm^{-1}.

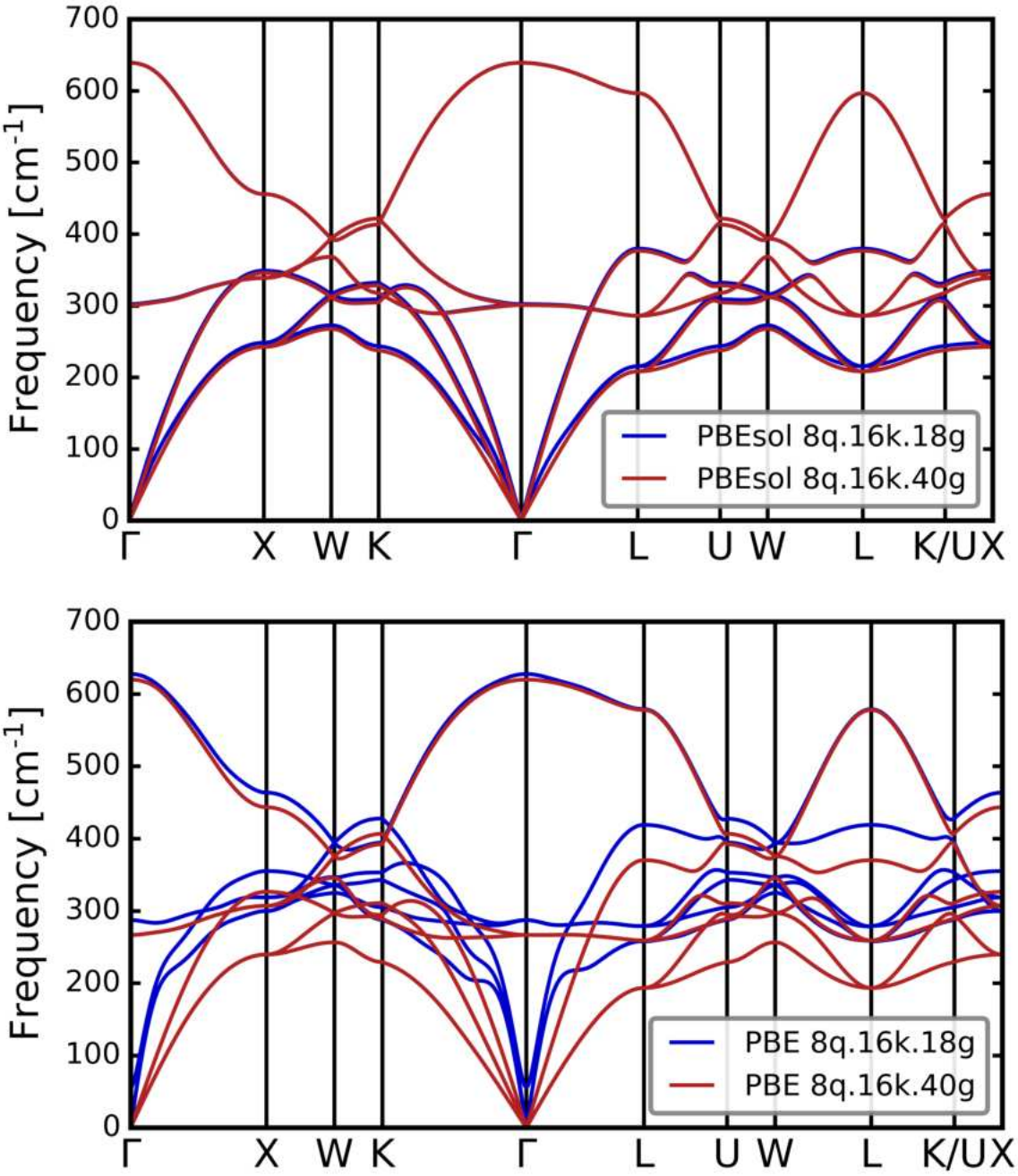

Figure 3.10: Comparison of the phonon calculations for LiF for `PBEsol` and `PBE`. Upper panel: Phonon-dispersion relations obtained for `PBEsol` with `8q.16k.18g` (blue lines) and `8q.16k.40g` (red lines). Lower panel: Same as the upper panel for `PBE`.

In particular, this may happen in some place belonging to the interstitial region. Increasing the value of **gmaxvr** increases the accuracy of the density description, thus improving the quality of the results.

The converged **PDR** for **PBEsol**, obtained with **8q.16k.40g**, can be compared with the results of other theoretical calculations. In particular, Fig. 3.11 shows the comparison of our results, rescaled in the size of the plot, with the first-principles **PDR** obtained using the pseudo-potential **abinit** code, taken from Ref. [35]. The agreement between the two **PDR** is very impressive.

Figure 3.12 shows a summary of the converged results obtained for LiF. The **PDR** and **PDOS** calculated with **LDA**, **PBEsol**, and **PBE** are qualitatively very similar, and as discussed in the case of Ge, the phonon frequencies show a well-defined trend when increasing the equilibrium unit-cell volume. Furthermore, Table 3.6 reports the values of the calculated phonon frequencies at the high-symmetry points Γ, X, and L for the different exchange-correlation functionals used in this work. These values are also compared with the experimental values of Ref. [34]. Finally, the converged values of the Born effective charges of Li and F as well as the clamped-nuclei dielectric constant are shown in Table 3.6 in comparison with the available experimental data [36].

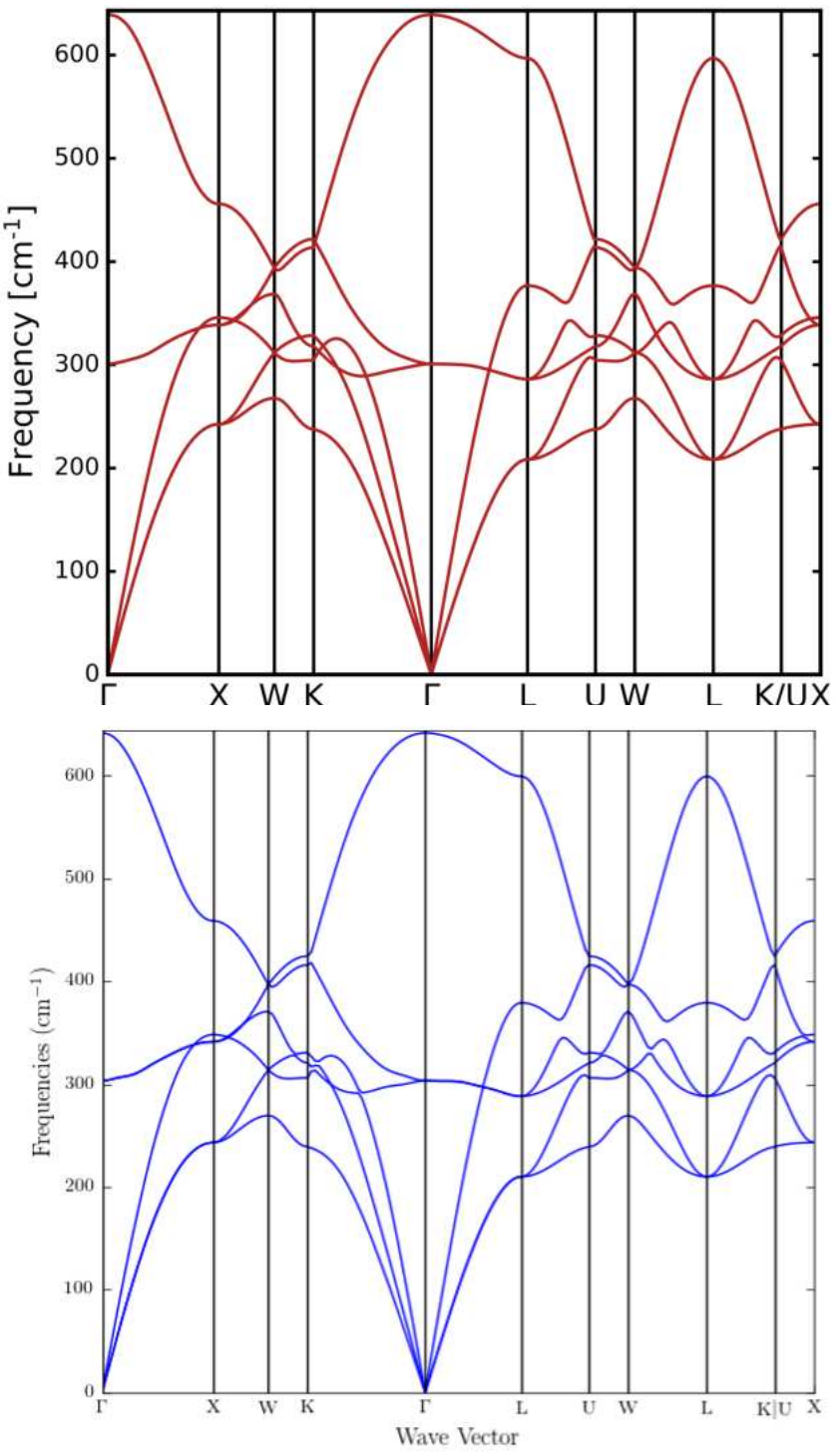

Figure 3.11: Comparison of the phonon calculations for LiF using `PBEsol`. Upper panel: Converged phonon-dispersion relations calculated in this work. Lower panel: Phonon-dispersion relations calculated using the **`abinit`** code, taken from Ref. [35].

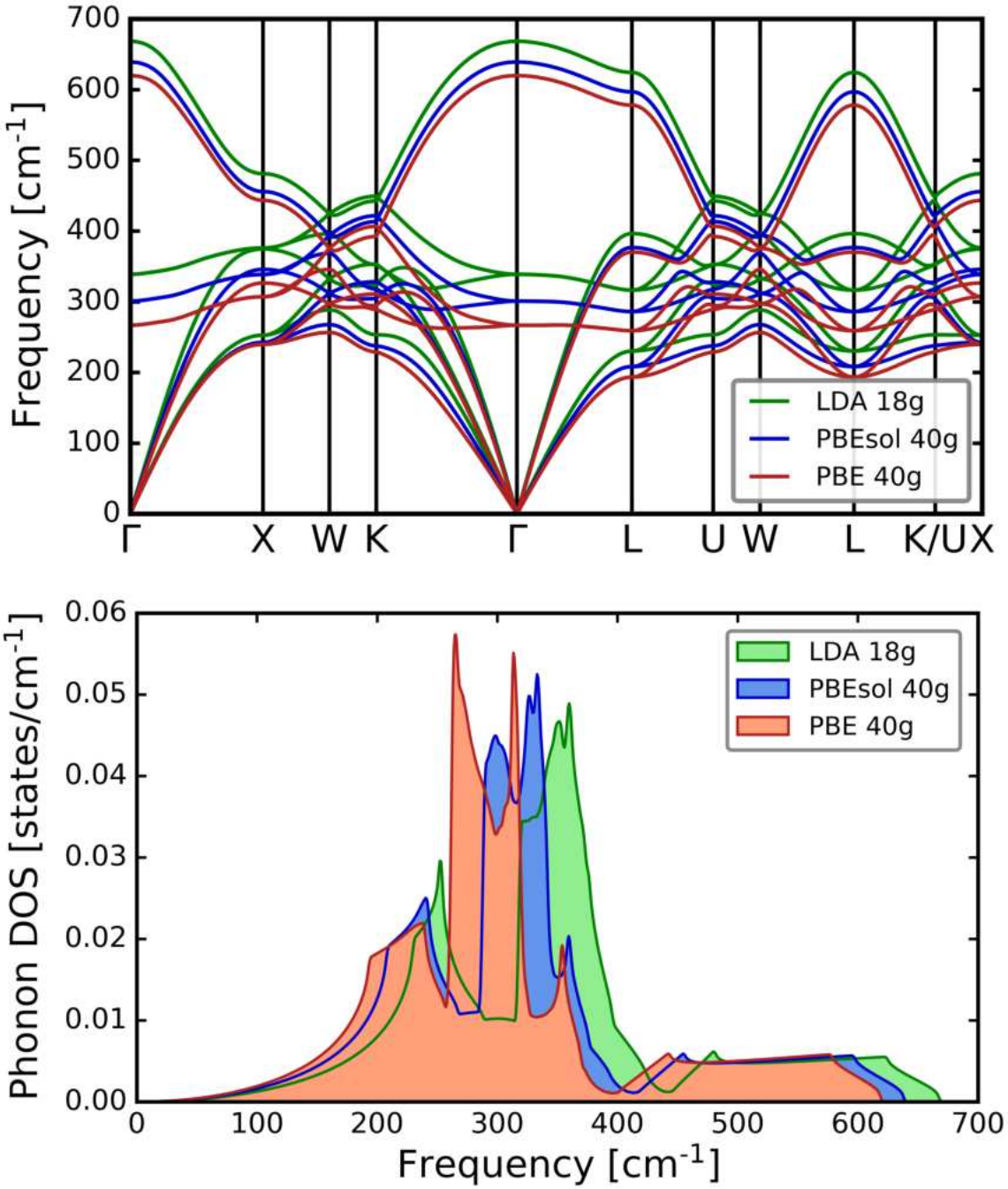

Figure 3.12: Comparison of the phonon calculations for LiF using `8q.16k.18g` for `LDA` and `8q.16k.40g` for `PBEsol` and `PBE`. Upper panel: Phonon-dispersion relations obtained with the `LDA` (green lines), `PBEsol` (blue lines), and `PBE` (red lines). Lower panel: Phonon density of states.

Table 3.7: Comparison of the calculated and experimental phonon frequencies of Ge, in units of cm^{-1}, for the high-symmetry points Γ, X, and L of the first Brillouin zone. In addition, the values of the converged Born effective charges for Li and F as well as the clamped-nuclei dielectric constant are shown in comparison to the available experiments.

	`LDA`	`PBEsol`	`PBE`	`Expt.`
Z^*_{Li}	1.041	1.049	1.055	
Z^*_{F}	-1.041	-1.049	-1.055	
ϵ^{∞}	2.114	2.085	2.047	1.93[a]
Γ_{TO}	339	301	267	305[b]
Γ_{LO}	668	639	620	657[b]
X_{TA}	253	242	240	257[b]
X_{LA}	375	345	326	350[b]
X_{TO}	376	338	307	345[b]
X_{LO}	481	456	443	457[b]
L_{TA}	230	208	193	207[b]
L_{LA}	396	377	370	387[b]
L_{TO}	316	286	259	300[b]
L_{LO}	624	597	578	630[b]

[a] Ref. [36]
[b] Ref. [34]

Chapter 4

Conclusions and Outlook

In this work, the phonon-dispersion relations, the phonon density of states, and the phonon frequencies for germanium and lithium fluoride were investigated. For this purpose, the density-functional theory and the density-functional perturbation theory, both implemented in the **exciting** code, were used for the calculations of the ground-states and the phonon properties. The first objective was to gain new data for the phonon properties of Ge and LiF. The second objective was to test and verify the linear-response approach within the density-functional perturbation theory in the **exciting** code.

For germanium, the **PDR** and **PDOS** can be considered as converged for **8q.16k**. The converged phonon properties show good agreement with both theoretical and experimental values present in the literature. For Ge, the calculations performed using **DFPT** showed untypical enhancement of the frequencies at the Γ point. To investigate this discrepancy, the phonon frequencies at high-symmetry points in the Brillouin zone were calculated using the super-cell (**sc**) method also implemented in **exciting**. These **sc** calculations are in full agreement with the **DFPT** ones, except at the Γ point, where more reasonable values are obtained using the **sc** method. This result gives indication that the implementation of the **DFPT** in **exciting** at $\mathbf{q} = 0$ should be revised. Calculations with **DFPT** and with the dynamical matrix replaced at Γ by the **sc** one were considered as converged.

Converged results for the **PDR** and **PDOS** of LiF can be also obtained by using **8q.16k**. Furthermore, the prototypical case of the ionic compound lithium fluoride gave us the opportunity to put in evidence the role of the numerical parameter **gmaxvr** for the determination of fully converged phonon properties. This parameter express the accuracy in the description of the electron density in the interstitial region. The use of large values of **gmaxvr**, well above the default ones, is crucial for calculations performed with **GGA** exchange-correlation functionals, which require an accurate numerical determination of the electron-density gradient.

For both germanium and lithium fluoride, it was found that the phonon-dispersion relations and the phonon density of states calculated with `LDA`, `PBEsol` and `PBE` are qualitatively very similar. However, for a fixed **k**-vector, the phonon frequencies are shifted against each other. The phonon frequencies for `LDA` are the highest and the ones for `PBE` are the lowest. The phonon frequencies for `PBEsol` lie between those. This behavior can be explained by the fact that different equilibrium lattice parameters result from the use of different exchange-correlation functionals. Calculations with different lattice parameters in turn lead to different phonon frequencies.

Bibliography

[1] "Germanium." chemie.de.
https://www.chemie.de/lexikon/Germanium.html
(accessed Aug. 02, 2024).

[2] "Diamantstruktur." chemie.de.
https://www.chemie.de/lexikon/Diamantstruktur.html
(accessed Aug. 02, 2024).

[3] "Natriumchlorid-Struktur." chemie.de.
https://www.chemie.de/lexikon/Natriumchlorid-Struktur.html
(accessed Aug. 02, 2024).

[4] "Lithiumfluorid." chemie.de
https://www.chemie.de/lexikon/Lithiumfluorid.html
(accessed Aug. 02, 2024).

[5] F. Giustino, *Materials Modelling Using Density-Functional Theory.* Oxford University Press, 2014.

[6] D. S. Sholl and J. A. Steckel, *Density-Functional Theory.* 2009. doi: 10.1002/9780470447710.

[7] A. Gulans, S. Kontur, C. Meisenbichler, D. Nabok, P. Pavone, S. Rigamonti, S. Sagmeister, U. Werner, and C. Draxl, "**exciting**: a full-potential all-electron package implementing density-functional theory and many-body perturbation theory," *Journal of physics. Condensed matter*, vol. 26, p. 363202, Aug. 2014. doi: 10.1088/0953-8984/26/36/363202.

[8] S. Tillack and P. Pavone, "Lattice Dynamics of Diamond and Zincblende-Structure Crystals." exciting-code.org.
http://exciting.wikidot.com/neon-lattic e-dynamics
(accessed Aug. 04, 2024).

[9] J. P. Perdew, A. Ruzsinszky, G. I. Csonka, O. A. Vydrov, G. E. Scuseria, L. A. Constantin, X. Zhou, and K. Burke, "Restoring the Density-Gradient Expansion for Exchange in Solids and Surfaces," *Physical review letters*, vol. 100, 4 2008. doi: 10.1103/physrevlett.100.136406.

[10] R. Gross and A. Marx, *Festkörperphysik*. 2014. doi: 10.1524/9783110358704.

[11] "Diamond - Molecule of the Month - July 1996 (HTML version)." chm.bris.ac.uk. https://www.chm.bris.ac.uk/motm/diamond/diamondh.html (accessed Aug. 02, 2024).

[12] M. McKay, "Optical studies of h-BN and ErN," 8 2021. https://ttu-ir.tdl.org/handle/2346/87878?show=fulllocale-attribute=es (accessed Aug. 02, 2024).

[13] G. Czycholl, *Theoretische Festkörperphysik Band 1*. 2016. doi: 10.1007/978-3-662-47141-8.

[14] P. Hohenberg and W. Kohn, "Inhomogeneous electron gas," *Physical Review*, vol. 136, pp. B864–B871, 11 1964. doi: 10.1103/physrev.136.b864.

[15] S. Tillack, P. Pavone, and C. Draxl. To be submitted (2024).

[16] P. Giannozzi, S. De Gironcoli, P. Pavone, and S. Baroni, "Ab-initio calculation of phonon dispersions in semiconductors," *Physical review. B, Condensed matter*, vol. 43, pp. 7231–7242, 3 1991. doi: 10.1103/physrevb.43.7231.

[17] S. Lubeck. Private communication.

[18] "Groundstate." exciting-code.org. http://exciting.wikidot.com/ref:groundstate (accessed Aug. 02, 2024).

[19] "Phonons." exciting-code.org. http://exciting.wikidot.com/ref:phonons (accessed Aug. 02, 2024).

[20] P. G. Risueno and P. Pavone, "Simple convergence tests." exciting-code.org. http://exciting.wikidot.com/neon-simple-convergence-tests (accessed Aug. 02, 2024).

[21] P. Pavone, "Volume optimization for cubic systems." exciting-code.org. http://exciting.wikidot.com/neon-volume-optimization-for-cubic-systems (accessed Aug. 02, 2024).

[22] F. Birch, "Finite Elastic Strain of Cubic Crystals," *Physical review*, vol. 71, pp. 809–824, 6 1947. doi: 10.1103/physrev.71.809.

[23] V. Fiorentini, "Semiconductor band structures at zero pressure," *Physical review. B, Condensed matter*, vol. 46, pp. 2086–2091, 7 1992. doi: 10.1103/physrevb.46.2086.

[24] C. Filippi, D. J. Singh, and C. J. Umrigar, "All-electron local-density and generalized-gradient calculations of the structural properties of semic onductors," *Physical review. B, Condensed matter*, vol. 50, pp. 14947–14951, 11 1994. 10.1103/physrevb.50.14947.

[25] P. Hao, Y. Fang, J. Sun, G. I. Csonka, P. H. T. Philipsen, and J. P. Perdew, "Lattice constants from semilocal density functionals with zero-point phonon correction," *Physical review. B, Condensed matter and materials physics*, vol. 85, 1 2012. doi: 10.1103/physrevb.85.014111.

[26] G. I. Csonka, J. P. Perdew, A. Ruzsinszky, P. H. T. Philipsen, S. Lebègue, J. Paier, O. A. Vydrov, and J. G. Ángyán, "Assessing the performance of recent density functionals for bulk solids," *Physical review. B, Condensed matter and materials physics*, vol. 79, 4 2009. doi: 10.1103/physrevb.79.155107.

[27] S. Ren, H. Yang, S. Singh, P. E. Batson, E. L. Garfunkel, and D. Vanderbilt, "Electronic structure of Humble defects in Ge and Ge0.8Si0.2," *Physical review. B./Physical review. B*, vol. 106, 10 2022. doi: 10.1103/physrevb.106.155302.

[28] T. Hom, W. Kiszenik, and B. Post, "Accurate lattice constants from multiple reflection measurements. II. Lattice constants of germanium silicon, and diamond," *Journal of applied crystallography*, vol. 8, pp. 457–458, 8 1975. doi: 10.1107/s0021889875010965.

[29] J. F. C. Baker and M. Hart, "An absolute measurement of the lattice parameter of germanium using multiple-beam X-ray diffractometry," *Acta crystallographica. Section A, Crystal physics, diffraction, theoretical and general crystallography*, vol. 31, pp. 364–367, 5 1975. doi: 10.1107/s0567739475000769.

[30] L. Lindsay, "Isotope scattering and phonon thermal conductivity in light atom compounds: LiH and LiF," *Physical review. B./Physical review. B*, vol. 94, 11 2016. doi: 10.1103/physrevb.94.174304.

[31] M. E. Straumanis and J. S. Shah, "Low temperature lattice parameters and expansion coefficients of AI2Au and LiF Gruneisen constants of LiF," *Zeitschrift*

für anorganische und allgemeine Chemie, vol. 391, pp. 79–85, 7 1972. doi: 10.1002/zaac.19723910110.

[32] K. Chruszcz-Lipska, E. Szostak, K. K. Zborowski, and E. Knapik, "Study of the Structure and Infrared Spectra of LiF, LiCl and LiBr Using Density Functional Theory (DFT)," *Materials*, vol. 16, p. 5353, 7 2023. doi: 10.3390/ma16155353.

[33] G. Nilsson and G. Nelin, "Phonon Dispersion Relations in Ge at 80 °K," *Physical review. B, Solid state*, vol. 3, pp. 364–369, 1 1971. doi: 10.1103/physrevb.3.364.

[34] G. Dolling, H. G. Smith, R. M. Nicklow, P. R. Vijayaraghavan, and M. K. Wilkinson, "Lattice Dynamics of Lithium Fluoride," *Physical Review*, vol. 168, pp. 970–979, 4 1968. doi: 10.1103/physrev.168.970.

[35] "mp-1138: LiF (cubic, Fm-3m, 225)." legacy.materialsproject.org. https://legacy.materialsproject.org/materials/mp-1138/ (accessed Aug. 02, 2024).

[36] R. Lowndes and D. Martin *Proc. Roy. Soc. A*, vol. 308, p. 473, 1969.

Appendix A

`species` files

This appendix lists the **`species`** files used for the elements Li, F, and Ge.

```
<?xml version="1.0" encoding="UTF-8"?>
<spdb xsi:noNamespaceSchemaLocation="../../xml/species.xsd"
      xmlns:xsi="http://www.w3.org/2001/XMLSchema-instance">
  <sp chemicalSymbol="Li" name="lithium" z="-3.00000" mass="12652.66897">
    <muffinTin rmin="0.100000E-04" radius="1.7000" rinf="29.9495"
               radialmeshPoints="250"/>
    <atomicState n="1" l="0" kappa="1" occ="2.00000" core="false"/>
    <atomicState n="2" l="0" kappa="1" occ="1.00000" core="false"/>
    <basis>
      <default type="lapw" trialEnergy="0.1500" searchE="false"/>
      <custom l="0" type="lapw" trialEnergy="0.1500" searchE="false"/>
      <lo l="0">
        <wf matchingOrder="0" trialEnergy="0.1500" searchE="false"/>
        <wf matchingOrder="1" trialEnergy="0.1500" searchE="false"/>
      </lo>
      <lo l="0">
        <wf matchingOrder="0" trialEnergy="0.15" searchE="false"/>
        <wf matchingOrder="2" trialEnergy="0.15" searchE="false"/>
      </lo>
      <lo l="0">
        <wf matchingOrder="0" trialEnergy="0.15" searchE="false"/>
        <wf matchingOrder="0" trialEnergy="-1.60" searchE="false"/>
      </lo>
      <lo l="0">
        <wf matchingOrder="0" trialEnergy="-1.60" searchE="false"/>
        <wf matchingOrder="1" trialEnergy="-1.60" searchE="false"/>
      </lo>
    </basis>
  </sp>
</spdb>
```

Figure A.1: **`species`** file for Li.

```
<?xml version="1.0" encoding="UTF-8"?>
<spdb xsi:noNamespaceSchemaLocation="../../xml/species.xsd"
      xmlns:xsi="http://www.w3.org/2001/XMLSchema-instance">
  <sp chemicalSymbol="F" name="fluorine" z="-9.00000" mass="34631.97043">
    <muffinTin rmin="0.100000E-05" radius="1.4500" rinf="15.7761"
               radialmeshPoints="400"/>
    <atomicState n="1" l="0" kappa="1" occ="2.00000" core="true"/>
    <atomicState n="2" l="0" kappa="1" occ="2.00000" core="false"/>
    <atomicState n="2" l="1" kappa="1" occ="2.00000" core="false"/>
    <atomicState n="2" l="1" kappa="2" occ="3.00000" core="false"/>
    <basis>
      <default type="lapw" trialEnergy="0.1500" searchE="false"/>
      <custom l="0" type="lapw" trialEnergy="-1.0" searchE="false"/>
      <lo l="0">
        <wf matchingOrder="0" trialEnergy="-1.0" searchE="false"/>
        <wf matchingOrder="1" trialEnergy="-1.0" searchE="false"/>
      </lo>
      <lo l="0">
        <wf matchingOrder="0" trialEnergy="-1.0" searchE="false"/>
        <wf matchingOrder="2" trialEnergy="-1.0" searchE="false"/>
      </lo>
      <lo l="0">
        <wf matchingOrder="0" trialEnergy="-1.0" searchE="false"/>
        <wf matchingOrder="3" trialEnergy="-1.0" searchE="false"/>
      </lo>

      <custom l="1" type="lapw" trialEnergy="0.15" searchE="false"/>
      <lo l="1">
        <wf matchingOrder="0" trialEnergy="0.15" searchE="false"/>
        <wf matchingOrder="1" trialEnergy="0.15" searchE="false"/>
      </lo>
      <lo l="1">
        <wf matchingOrder="0" trialEnergy="0.15" searchE="false"/>
        <wf matchingOrder="2" trialEnergy="0.15" searchE="false"/>
      </lo>
      <lo l="1">
        <wf matchingOrder="0" trialEnergy="0.15" searchE="false"/>
        <wf matchingOrder="3" trialEnergy="0.15" searchE="false"/>
      </lo>
      <custom l="2" type="lapw" trialEnergy="0.15" searchE="false"/>
      <lo l="2">
        <wf matchingOrder="0" trialEnergy="0.15" searchE="false"/>
        <wf matchingOrder="1" trialEnergy="0.15" searchE="false"/>
      </lo>
      <lo l="2">
        <wf matchingOrder="0" trialEnergy="0.15" searchE="false"/>
        <wf matchingOrder="2" trialEnergy="0.15" searchE="false"/>
      </lo>
      <custom l="3" type="lapw" trialEnergy="0.15" searchE="false"/>
      <lo l="3">
        <wf matchingOrder="0" trialEnergy="0.15" searchE="false"/>
        <wf matchingOrder="1" trialEnergy="0.15" searchE="false"/>
      </lo>
      <lo l="3">
        <wf matchingOrder="0" trialEnergy="0.15" searchE="false"/>
        <wf matchingOrder="2" trialEnergy="0.15" searchE="false"/>
      </lo>

    </basis>
  </sp>
</spdb>
```

Figure A.2: `species` file for F.

```
<?xml version="1.0" encoding="UTF-8"?>
<spdb xsi:noNamespaceSchemaLocation="../../xml/species.xsd"
      xmlns:xsi="http://www.w3.org/2001/XMLSchema-instance">
  <sp chemicalSymbol="Ge" name="germanium" z="-32.0000" mass="132359.9329">
    <muffinTin rmin="0.100000E-05" radius="1.80000" rinf="25.3660"
               radialmeshPoints="800"/>
    <atomicState n="1" l="0" kappa="1" occ="2.00000" core="true"/>
    <atomicState n="2" l="0" kappa="1" occ="2.00000" core="true"/>
    <atomicState n="2" l="1" kappa="1" occ="2.00000" core="true"/>
    <atomicState n="2" l="1" kappa="2" occ="4.00000" core="true"/>
    <atomicState n="3" l="0" kappa="1" occ="2.00000" core="false"/>
    <atomicState n="3" l="1" kappa="1" occ="2.00000" core="false"/>
    <atomicState n="3" l="1" kappa="2" occ="4.00000" core="false"/>
    <atomicState n="3" l="2" kappa="2" occ="4.00000" core="false"/>
    <atomicState n="3" l="2" kappa="3" occ="6.00000" core="false"/>
    <atomicState n="4" l="0" kappa="1" occ="2.00000" core="false"/>
    <atomicState n="4" l="1" kappa="1" occ="1.00000" core="false"/>
    <atomicState n="4" l="1" kappa="2" occ="1.00000" core="false"/>
    <basis>
      <default type="lapw" trialEnergy="0.1500" searchE="false"/>
      <custom l="0" type="lapw" trialEnergy="0.1500" searchE="false"/>
      <lo l="0">
        <wf matchingOrder="0" trialEnergy="0.1500" searchE="false"/>
        <wf matchingOrder="1" trialEnergy="0.1500" searchE="false"/>
      </lo>
      <lo l="0">
        <wf matchingOrder="0" trialEnergy="0.1500" searchE="false"/>
        <wf matchingOrder="0" trialEnergy="-6.2" searchE="false"/>
      </lo>
      <lo l="0">
        <wf matchingOrder="0" trialEnergy="-6.2" searchE="false"/>
        <wf matchingOrder="1" trialEnergy="-6.2" searchE="false"/>
      </lo>
      <lo l="0">
        <wf matchingOrder="0" trialEnergy="-6.2" searchE="false"/>
        <wf matchingOrder="2" trialEnergy="-6.2" searchE="false"/>
      </lo>
      <custom l="1" type="lapw" trialEnergy="0.1500" searchE="false"/>
      <lo l="1">
        <wf matchingOrder="0" trialEnergy="0.1500" searchE="false"/>
        <wf matchingOrder="1" trialEnergy="0.1500" searchE="false"/>
      </lo>
      <lo l="1">
        <wf matchingOrder="0" trialEnergy="0.1500" searchE="false"/>
        <wf matchingOrder="0" trialEnergy="-4.18619964259" searchE="false"/>
      </lo>
      <lo l="1">
        <wf matchingOrder="0" trialEnergy="-4.18619964259" searchE="false"/>
        <wf matchingOrder="1" trialEnergy="-4.18619964259" searchE="false"/>
      </lo>
      <lo l="1">
        <wf matchingOrder="0" trialEnergy="-4.18619964259" searchE="false"/>
        <wf matchingOrder="2" trialEnergy="-4.18619964259" searchE="false"/>
      </lo>
      <custom l="2" type="lapw" trialEnergy="-1.07588667005" searchE="false"/>
      <lo l="2">
        <wf matchingOrder="0" trialEnergy="-1.07588667005" searchE="false"/>
        <wf matchingOrder="1" trialEnergy="-1.07588667005" searchE="false"/>
      </lo>
      <lo l="2">
        <wf matchingOrder="0" trialEnergy="-1.07588667005" searchE="false"/>
        <wf matchingOrder="2" trialEnergy="-1.07588667005" searchE="false"/>
      </lo>
    </basis>
  </sp>
</spdb>
```

Figure A.3: `species` file for Ge.

Appendix B

Phonon properties of Ge

This appendix shows the converged phonon-dispersion relations and phonon density of states of germanium for all exchange-correlation functional considered in this thesis. All calculation were performed using `8r.18g` and `0.01s`. For the interpolation of the phonon-dispersion relations the dynamical matrix at the Γ point calculated using `DFPT` was replaced by the one obtained with the supercell method using the same computational parameters. Figures B.1, B.2, and B.3 show the results obtained using the `LDA`, `PBEsol`, and `PBE` exchange-correlation functional, respectively.

B.1 LDA

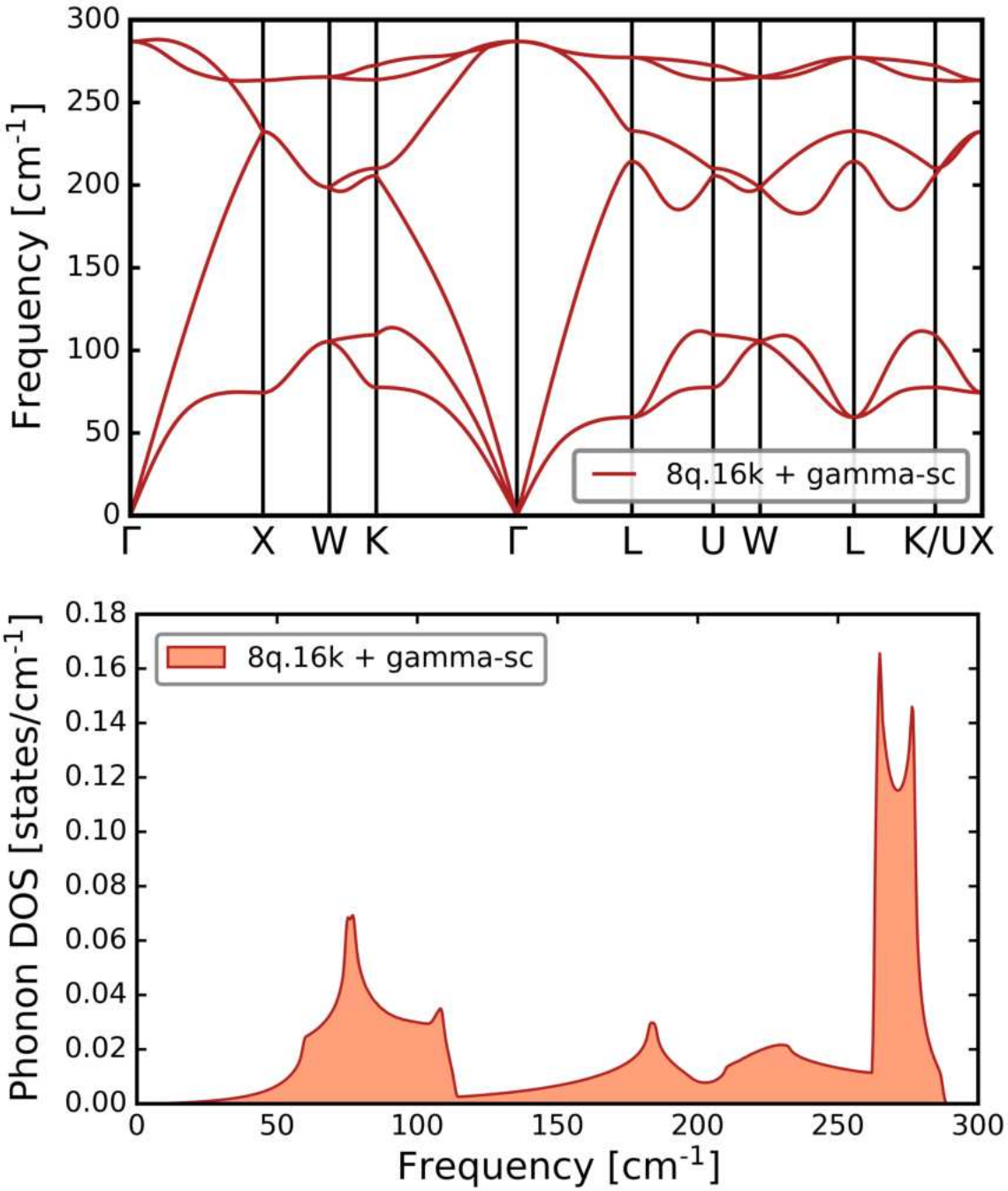

Figure B.1: Converged results of the `LDA` phonon calculations for Ge. Upper panel: Phonon-dispersion relations for `8q.16k`. Lower panel: Phonon density of states.

B.2 `PBEsol`

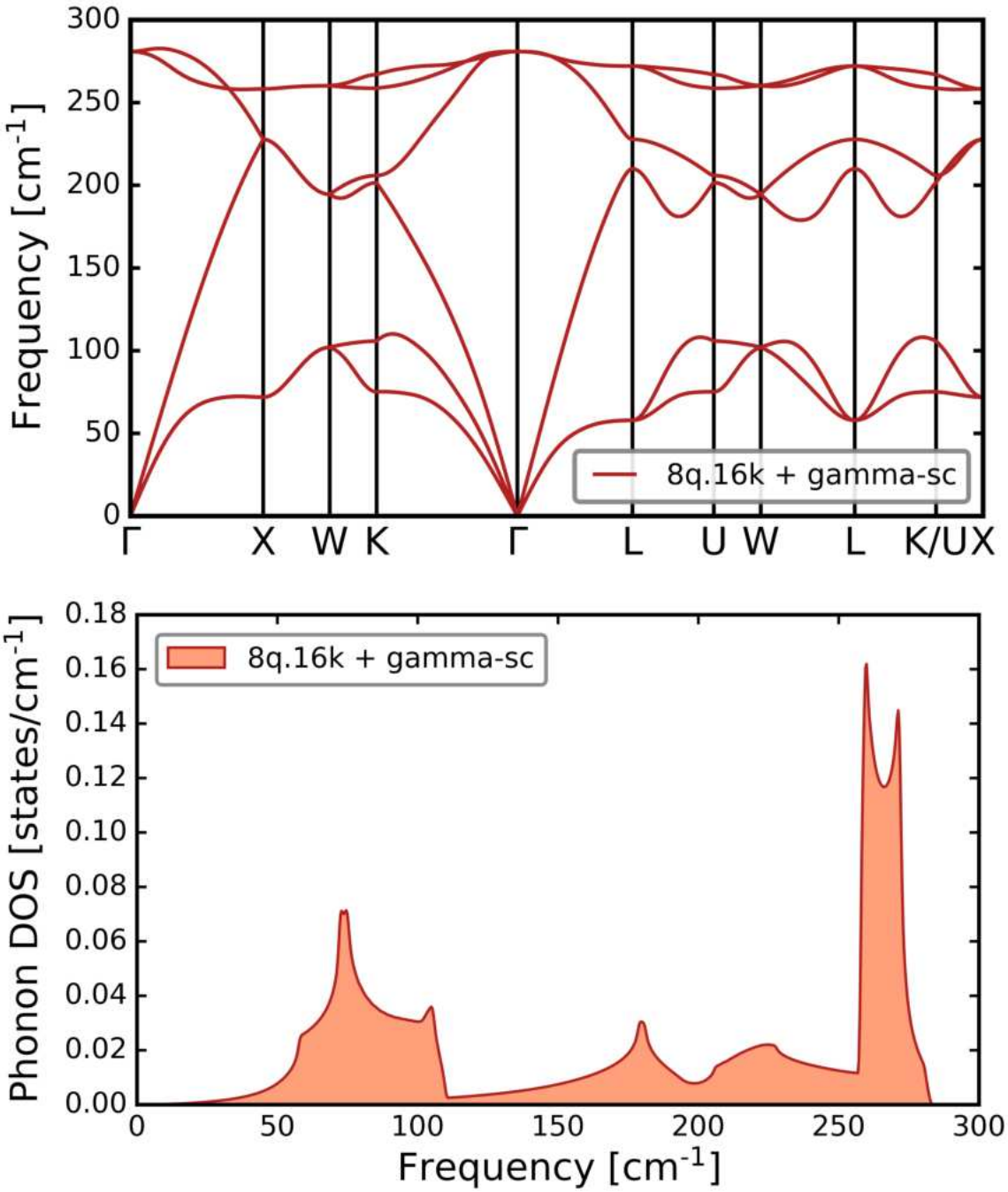

Figure B.2: Converged results of the `PBEsol` phonon calculations for Ge. Upper panel: Phonon-dispersion relations for `8q.16k`. Lower panel: Phonon density of states.

B.3 PBE

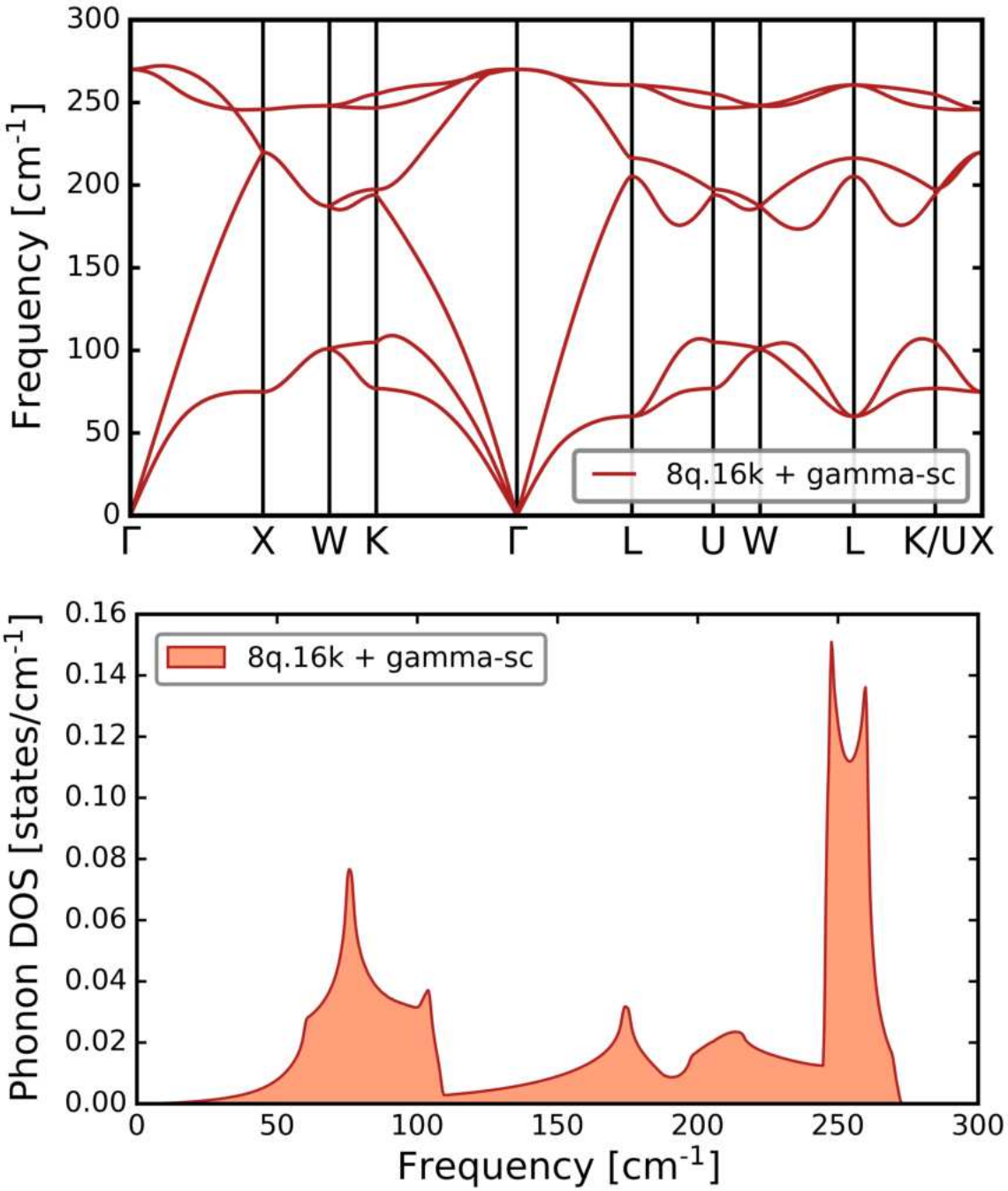

Figure B.3: Converged results of the `PBE` phonon calculations for Ge. Upper panel: Phonon-dispersion relations for `8q.16k`. Lower panel: Phonon density of states.

Appendix C

Phonon properties of LiF

This appendix shows the converged phonon-dispersion relations and phonon density of states of lithium fluoride for all exchange-correlation functional considered in this thesis. All calculation were performed using `8r` and `0.0001s`. Figures C.1, C.2, and C.3 show the results obtained using the `LDA`, `PBEsol`, and `PBE` exchange-correlation functional, respectively.

C.1 LDA

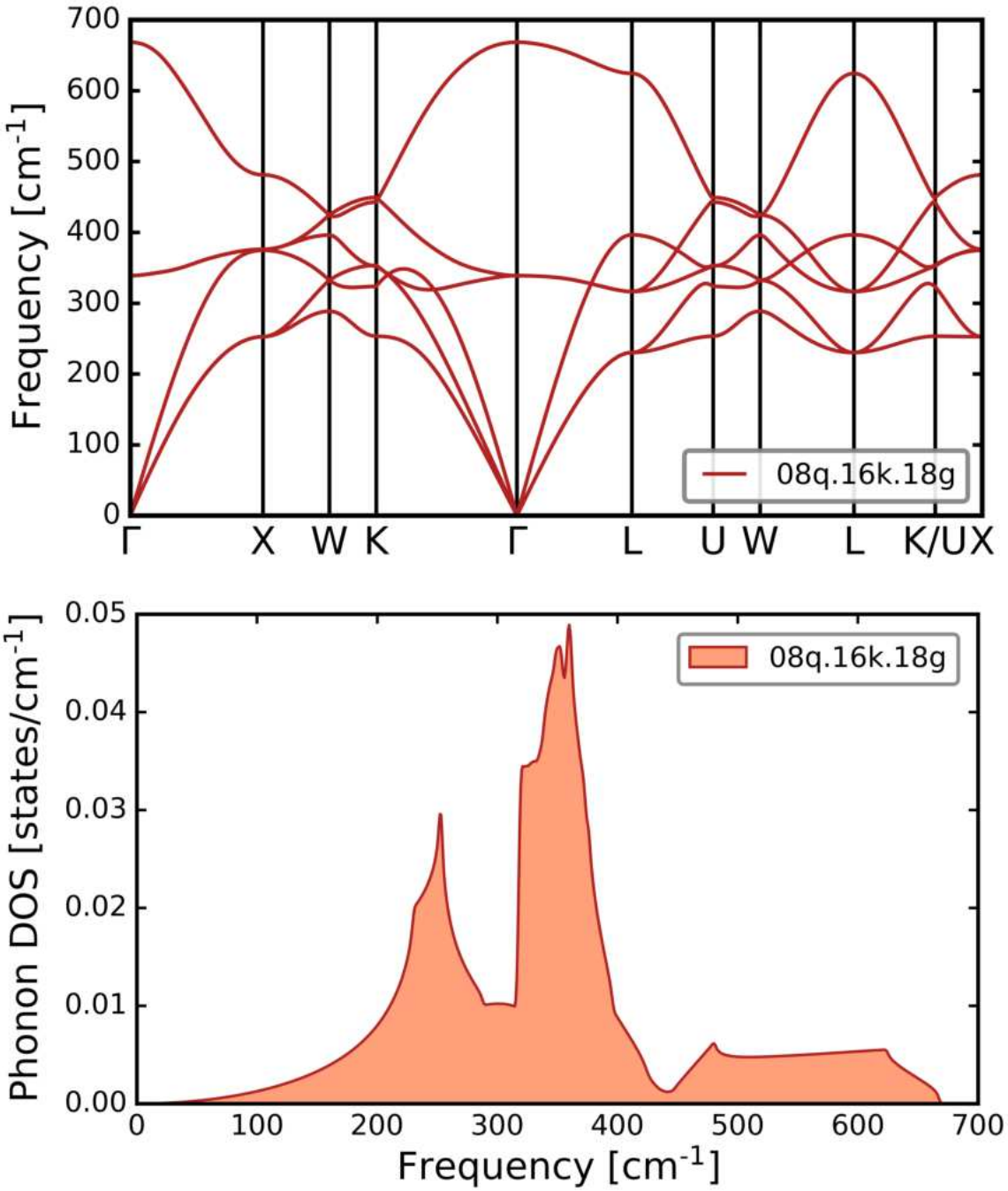

Figure C.1: Converged results of the `LDA` phonon calculations for LiF. Upper panel: Phonon-dispersion relations for `8q.16k.18g`. Lower panel: Phonon density of states.

C.2 `PBEsol`

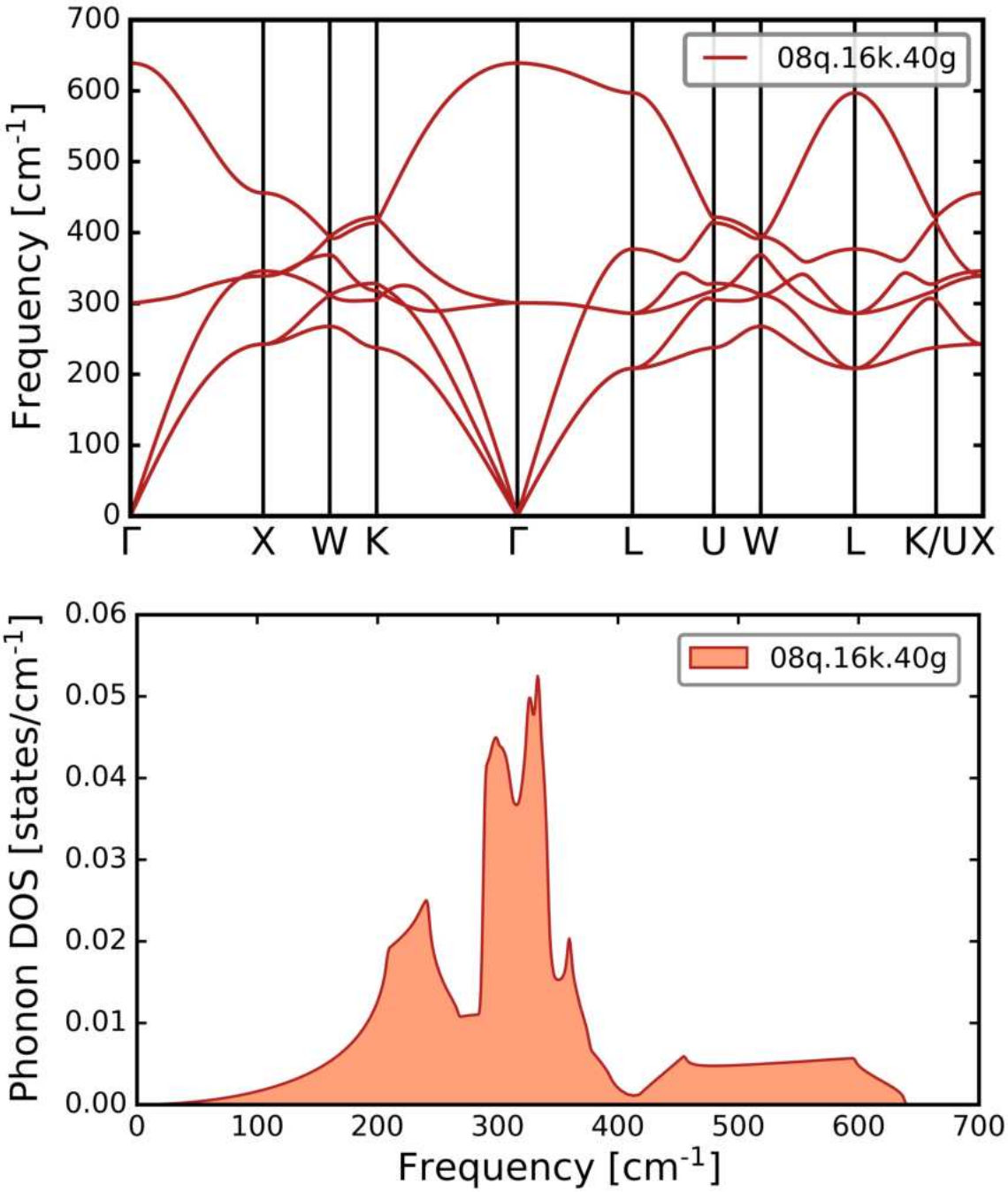

Figure C.2: Converged results of the `PBEsol` phonon calculations for LiF. Upper panel: Phonon-dispersion relations for `8q.16k.40g`. Lower panel: Phonon density of states.

C.3 PBE

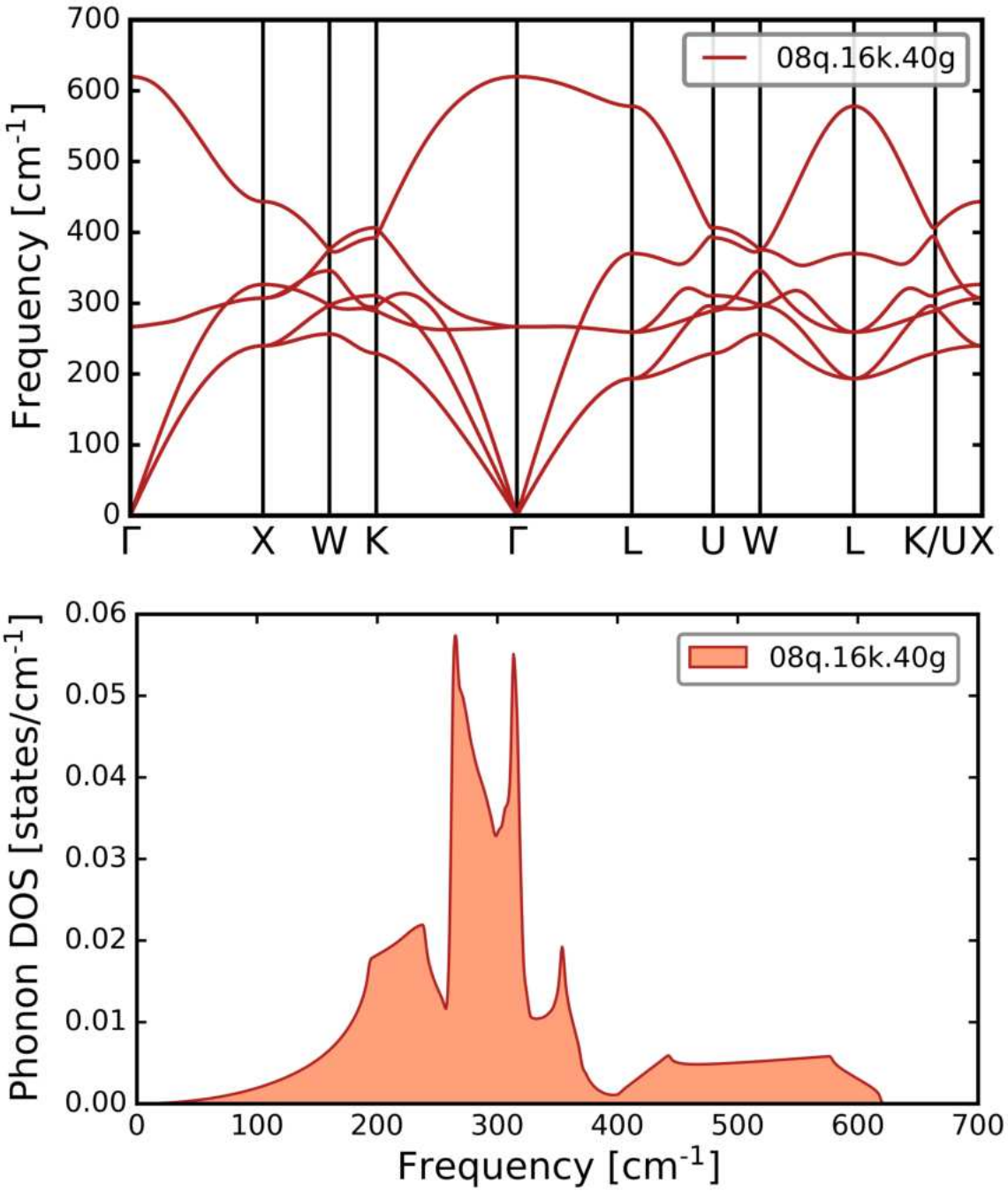

Figure C.3: Converged results of the `PBE` phonon calculations for LiF. Upper panel: Phonon-dispersion relations for `8q.16k.40g`. Lower panel: Phonon density of states.

Acknowledgments

First of all, I would like to thank my mother, whose support has made it possible for me to study under very good conditions. I would also like to thank Pasquale Pavone, who guided me through my Bachelor's thesis and always found the time to help me with problems. I would also like to thank Sven Lubeck, who provided the `species` files for the elements.

Selbstständigkeitserklärung

Ich erkläre hiermit, dass ich die vorliegende Arbeit selbstständig verfasst und noch nicht für andere Prüfungen eingereicht habe. Sämtliche Quellen einschließlich Internetquellen, die unverändert oder abgewandelt wiedergegeben werden, insbesondere Quellen für Texte, Grafiken, Tabellen, Bilder sowie die Nutzung von Künstlicher Intelligenz für die Erstellung von Texten und Abbildungen, sind als solche kenntlich gemacht. Mir ist bekannt, dass bei Verstößen gegen diese Grundsätze ein Verfahren wegen Täuschungsversuchs bzw. Täuschung eingeleitet wird.

Berlin, 03.09.2024

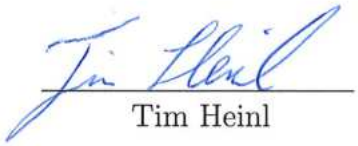

Tim Heinl